NASA TECHNICAL MEMORANDUM

NASA TM X-1589

NASA TM X-1589

ANALYTICAL INVESTIGATION OF EFFECTS OF PHYSICAL AND AERODYNAMIC PARAMETERS ON DYNAMIC BEHAVIOR OF PROJECT FIRE REENTRY VEHICLE

by Jacob H. Lichtenstein

Langley Research Center

Langley Station, Hampton, Va.

NATIONAL AERONAUTICS AND SPACE ADMINISTRATION • WASHINGTON, D. C. • JUNE 1968

NASA TM X-1589

ANALYTICAL INVESTIGATION OF EFFECTS OF PHYSICAL AND AERODYNAMIC PARAMETERS ON DYNAMIC BEHAVIOR OF PROJECT FIRE REENTRY VEHICLE

By Jacob H. Lichtenstein

Langley Research Center
Langley Station, Hampton, Va.

NATIONAL AERONAUTICS AND SPACE ADMINISTRATION

For sale by the Clearinghouse for Federal Scientific and Technical Information
Springfield, Virginia 22151 – CFSTI price $3.00

ANALYTICAL INVESTIGATION OF EFFECTS OF PHYSICAL AND AERODYNAMIC PARAMETERS ON DYNAMIC BEHAVIOR OF PROJECT FIRE REENTRY VEHICLE

By Jacob H. Lichtenstein
Langley Research Center

SUMMARY

The heat-transfer characteristics of a body entering the earth's atmosphere at superorbital velocities are important in the consideration of any planetary mission. In an attempt to measure these characteristics experimentally, Project Fire was undertaken. During the design phase of the reentry vehicle, information was necessary as to whether certain physical and aerodynamic parameters would become important design considerations. Consequently, an analytical study was undertaken to evaluate the effects of these parameters on the dynamic behavior of the reentry vehicle.

The results of the investigation showed that changes in most of the parameters considered, for instance, ±21 percent in the moments of inertia and ±50 percent in the spin rate, would not affect the dynamic behavior during the main heat-measuring period (the first 40 seconds) enough to cause serious design problems. However, mass-distribution asymmetry that would displace the center of gravity 1/8 inch (0.003 meter) or more from the vehicle axis of symmetry would create angle-of-attack disturbances large enough to be significant.

INTRODUCTION

The heat-transfer characteristics of a body entering the earth's atmosphere at superorbital velocities are important in the consideration of a lunar mission such as Apollo. In an attempt to measure these heat-transfer characteristics experimentally, Project Fire was undertaken. Briefly, this project consisted of lofting a vehicle similar in shape to the Apollo command module above the atmosphere and then, during its return toward earth, increasing its velocity with the aid of a rocket to about 37 000 ft/sec (11 278 m/sec). Early in the Project Fire program, it was recognized that certain physical, aerodynamic, and initial trajectory parameters could seriously affect the behavior of the reentry vehicle and thus its primary purpose of heat-transfer measurement. Therefore, an analytical program of computations on a digital electronic computer was undertaken to determine the effects on the reentry behavior of changes in such things as the

moments of inertia, spin rate, center-of-gravity location, initial angle of attack and initial pitch angle, and aerodynamic parameters. In order to obtain some of this information quickly, computations were first made with an existing program which necessitated maintaining the aerodynamic and mass data constant during a trajectory computation. The computation program was subsequently revised to permit variation of the center-of-gravity location and to include moment disturbances that were not available in the original program.

The data presented in this paper are the results of this analytical investigation to evaluate the effects of the changes in physical and aerodynamic parameters on the dynamic behavior of the Project Fire reentry vehicle. Inasmuch as the data generated in the computations were mainly for information input to Project Fire, they are presented without a detailed analysis of their significance.

SYMBOLS

The axis systems used in the present analysis are shown in figure 1. Because of the symmetry of the vehicle about the longitudinal axis, the forces and moments in the pitch and yaw planes are identical. The symbols used are defined in the following list. Physical quantities are given both in U.S. Customary Units and in the International System of Units (SI).

A cross-sectional reference area, feet^2 (meters^2)

A_{V_a} deceleration along the flight path, g units

$C_m = -C_n$ aerodynamic moment coefficient, $\frac{\text{Moment}}{q_p A d}$

$(C_m)_{p,\eta} = (C_n)_{p,\eta}$ Magnus moment coefficient, $\frac{\text{Magnus moment}}{q_p A d}$, per degree

$C_{m_q} = -C_{n_r}$ aerodynamic damping-moment coefficient, $\frac{\partial C_m}{\partial \frac{qd}{2V_a}}$ or $\frac{\partial C_n}{\partial \frac{rd}{2V_a}}$

$C_{m_\eta} = -C_{n_\eta}$ rate of change of aerodynamic moment coefficient with resultant angle of attack (static-stability coefficient), $\frac{\partial C_m}{\partial \eta}$ or $\frac{\partial (-C_n)}{\partial \eta}$, per radian

C_X aerodynamic axial-force coefficient, $\frac{\text{Axial force}}{q_p A}$

$C_Y = C_Z$ aerodynamic transverse-force coefficient, $\frac{\text{Transverse force}}{q_p A}$

C_{Yb}, C_{Zb}	applied-force coefficients along the body Y_b- and Z_b-axis
$C_{Y_\eta} = C_{Z_\eta}$	rate of change of transverse-force coefficient with resultant angle of attack, $\frac{\partial C_Y}{\partial \eta}$ or $\frac{\partial C_Z}{\partial \eta}$, per radian or per degree
d	reference length (diameter), feet (meters) (see fig. 2)
F_g	force due to gravity, pounds (newtons)
g	acceleration due to gravity on the earth's surface, 32.174 feet/second^2 (9.807 meters/second^2)
h	altitude, feet (meters)
I_X	moment of inertia about the X-axis, slug-feet^2 (kilogram-meters^2)
$I_Y = I_Z$	moments of inertia about the transverse axes, Y- and Z-axis, slug-feet^2 (kilogram-meters^2)
l	lateral distance between the center of pressure and the center of gravity, measured along the Y_b-axis, feet (meters)
M_{Yb}, M_{Zb}	moments applied about the body Y_b- and Z_b-axis, foot-pounds (newton-meters)
m	mass of the vehicle, slugs (kilograms)
p,q,r	rates of rotation about the X-, Y-, and Z-axis, radians/second
p_b, q_b, r_b	rates of rotation about the X_b-, Y_b-, and Z_b-axis, radians/second or degrees/second
q_p	dynamic pressure, $\frac{1}{2}\rho V_a^2$, pounds/foot^2 (newtons/meter^2)
r	radial distance from center of earth to center of gravity of vehicle, feet (meters)
r_e	equatorial radius of earth, 20 925 738 feet (6 378 165 meters)
t	time, seconds

u,v,w	velocities along the X-, Y-, and Z-axis, feet/second (meters/second)
V_a	resultant aerodynamic velocity, feet/second (meters/second)
V_i	resultant inertial velocity, feet/second (meters/second)
X,Y,Z	modified body-axis system in which Z remains in a plane parallel to the equatorial plane
x,y,z	distances along the X-, Y-, and Z-axis, feet (meters)
X_b,Y_b,Z_b	body-axis system
X_i,Y_i,Z_i	inertial-axis system, in which X_i and Z_i are in the plane of the equator and Y_i is positive toward the North Pole
x_i,y_i,z_i	distances along the X_i-, Y_i-, and Z_i-axis, feet (meters)
γ	flight-path angle with respect to local horizontal, degrees
η	resultant angle of attack with respect to flight path, degrees or radians
$\overline{\theta}$	angle between X_iZ_i-plane and location vector to vehicle (latitude), degrees
ρ	density of air, slugs/foot^3 (kilograms/meter^3)
ϕ,ψ,θ	Euler angles as defined in figure 1, in which the angles ψ and θ represent pitch and yaw, respectively, degrees
$\overline{\psi}$	angle in X_iZ_i-plane between X_iY_i-plane and plane containing vehicle (west longitude), degrees

Subscript:

o	at start of run

A dot over a symbol represents differentiation with respect to time.

GENERAL CONSIDERATIONS

The axis systems used in the analysis are shown in figure 1. Since the primary purpose of this study was to investigate the effects of various physical and aerodynamic parameters on the dynamic behavior of the reentry vehicle, the earth's spin and the actual longitude and latitude of the impact point were not considered. Therefore, the value of $\overline{\theta}$ was initially made zero so that the trajectories were essentially in the equatorial plane. Because of this orientation, the Euler angle ψ lies in the equatorial plane and represents the pitch angle, whereas the angle θ represents the out-of-plane or yaw angle.

In order to obtain some of the needed information quickly, the initial computations were made with an existing computer program, called the original program. This program had no provision for varying the mass and aerodynamic data during a trajectory computation. Therefore, the runs were made with constant mass and aerodynamic characteristics that represented average values during a descent. Because the flight vehicle was designed to spin at a relatively high rate (3 rps or 18.84 rad/sec), it would be made as symmetrical as possible. Therefore, for most of the runs, it was assumed that the vehicle would be symmetrical about the longitudinal axes $(I_Y = I_Z)$ and that the center of gravity generally would lie on the longitudinal (X) axis. The original computation program was subsequently modified to permit varying the center-of-gravity location and to include other parameters (such as Magnus moment coefficient, static-stability coefficient, and tipoff moment) required to provide information necessary to the Project Fire personnel. The equations of motion for this program, which is called the revised program, are presented in the appendix. They form a system of 5 degrees of freedom, with the roll rate specified constant throughout a run. The values used in this study for the various vehicle parameters are presented in tables I, II, and III, and a sketch of the reentry vehicle is shown in figure 2.

RESULTS AND DISCUSSION

Because the vehicle was symmetrical about the longitudinal axis, the angle-of-attack data presented are for the resultant or total angles of attack. They will be referred to simply as angles of attack throughout the remainder of the paper. Most of the figures that present angle-of-attack data are in two parts, the first showing the entire time history and the second showing approximately the first 50 seconds in greater detail. This early part of the run is the main heating period and thus is of primary interest. In order to save computer time, some of the trajectory computations were not carried through to completion. Once the pattern had been established, the computations for these cases were

stopped. It is convenient to divide the results into two groups, those obtained with the original program and those obtained with the revised program.

Results Obtained With Original Program

The present investigation was made primarily to evaluate the dynamic behavior of the reentry vehicle in response to various physical parameters. The effects investigated with the original program were those resulting from changes from the basic-case values (listed in table II) of ±21 percent in the moments of inertia and ±50 percent in the spin rate, changes in the initial angle of attack and initial pitch angle, and changes in the aerodynamic damping-moment coefficient. During the investigation, it was found that the variations over the ranges of the physical parameters produced only minor variations in the basic trajectory characteristics, such as velocity, altitude, and flight-path angle. Therefore, these results are presented only for the basic case and are considered applicable to all the cases. The data, presented in figures 3 and 4, are generally typical of most blunt-body reentry data, in that they exhibit a rapid decrease in velocity when an appreciable atmospheric density is reached, and a sharp knee in the curve of altitude variation with range (fig. 4) when speeds are low and the flight path becomes nearly vertical ($\gamma = -90^{o}$). Because the entry velocity of 37 000 ft/sec (11 278 m/sec) is above the orbital velocity of about 25 000 ft/sec (7620 m/sec), the flight-path angle with respect to the local horizontal actually becomes smaller in absolute value during the initial 30 seconds of the flight until the velocity has decreased to about orbital values. (See fig. 3(a).) The deceleration values are quite high (fig. 3(c)), reaching a maximum value of 75g and remaining above 50g for about 10 seconds.

Basic case.- The angle-of-attack variation with time for the basic case (run 1 in table II) is shown in figure 5. The triple lines in figure 5(b) show the magnitude of the angle-of-attack envelope and the mean values. The envelope is quite narrow and therefore blends into the one line for the scale used in figure 5(a). During the early part of the reentry, the angle of attack gradually increases because the vehicle, being spin stabilized, remains in its inertial attitude while the trajectory, as a result of the range angle traversed, gradually curves downward under it. The angle of attack and also the dynamic pressure increase until at about 14 seconds, the resulting aerodynamic moment is sufficient to perturb the vehicle from its original attitude. Because of the gyroscopic couple due to the spin rate, a precessional motion develops about the flight path. This circular motion can be seen in figure 6 for some representative time periods during the basic run.

Returning to figure 5, at about 33 seconds, where the peak dynamic pressure is passed and the flight-path angle begins to increase negatively, the angle of attack begins to increase rapidly, and at about 120 seconds, where the trajectory is nearly vertical, the angle of attack is about 90^{o}. At this time, the vehicle is nearly horizontal and is precessing about the vertical flight path with an angle of attack of almost 90^{o}.

The relatively slow development of the precessional motion can be seen from the time marks in figure 6. In this figure, ψ and θ are the pitch and yaw angles, respectively, measured from an axis system alined with the vertical and horizontal at $t = 0$ second and $h = 400\,000$ feet (122 000 meters). It can be seen that at about 10 seconds the vehicle has moved only about 0.01° in yaw, which amounts to a precessional angle of less than 1°. At 15 seconds the vehicle has precessed only about 35°, but after this time the precessional rate increases rapidly (see fig. 7), until at about 30 seconds the rate is nearly 3 rps. The displacement of the centers of the precessional circles shows the declination of the flight path from its initial value. The variation of the precessional rate with time almost directly parallels the dynamic-pressure variation.

In addition to the angle-of-attack variation, the angular rates and linear accelerations about and along the transverse body axes are of interest in order to insure that instruments of adequate range will be selected. In figure 8, the envelopes of the body yawing and pitching rates are presented. The shape of these curves is dictated by a combination of the dynamic-pressure and angle-of-attack variations with time. The body rates start to build up at about the time the precessional rate develops (at about 15 seconds). The first maximum in the rates occurs at about 40 seconds and is due mainly to the high precessional rate caused by the peak dynamic pressure. Between 50 and 80 seconds, the body rates decrease because the precessional rate has decreased (fig. 7) and the angle of attack (fig. 5) has not yet become very large. After this time, even though the precessional rate is low, the magnitude of the angle of attack becomes very large, and a large body rate results. Near the end of the trajectory, where the angles of attack for all the conditions are almost uniformly large and the precessional rate is nearly constant, all the body rates also have almost the same large magnitude. The actual body rates oscillate between the limits shown in figure 8 because the vehicle is spinning at 3 rps. In the early part of the trajectory, when there is a high precessional rate in addition to the spin, the oscillations are very rapid; however, near the end of the trajectory, when the precession is slow, the oscillations decrease in frequency to about 3 per second.

Effect of initial pitch angle and initial angle of attack.- Nominal values of the initial pitch angle and the initial angle of attack were -14.7° and 0°, respectively. Computations were made to assess the effect of slight changes from these values. The angle-of-attack variations with time are shown in figure 9 and the body-rate variations are shown in figure 10.

Each curve in figure 9 represents the mean angles of attack during the precession. This representation is acceptable because the angle of attack did not vary much during a precessional cycle, as can be seen from the near-circular nature of the curves in figure 6 which show the variation of ψ with θ for the basic case. When the initial angle of

attack of 1° is obtained by pitching the vehicle upward with respect to the trajectory (figs. 9(a) and (b)), the curves are similar to the basic-case curves, but are displaced to higher angle-of-attack values throughout most of the trajectory. When the initial angle of attack of 1° is obtained by pitching the vehicle downward, the angle of attack initially decreases, because of the trajectory curvature, to a value actually smaller than the basic-case values, then follows the same pattern as the other trajectories. It can be seen from the data that during the first 30 seconds, when the heating rate is maximum, and for about 10 seconds thereafter, the angle of attack barely exceeds the initial angle of attack. When the magnitude of the initial angle of attack is relatively large (5°), the pattern of results is similar to that for the 1° data, but is shifted upward. At the time of the writing only the $\eta_0 = 5^{\circ}$, with the vehicle pitched downward with respect to the trajectory (5° down) was available for presentation. The curve for $\eta_0 = 5^{\circ}$ down remained above the basic-case curve for the entire trajectory, whereas the curve for $\eta_0 = 1^{\circ}$ down was below the basic-case curve for most of the trajectory. This results from the fact that although the curvature of the trajectory reduced the magnitude of the angle of attack from its initial value of 5° down, the reduction was not enough, in this case, to reduce the angle below that for the basic case as it did for the case of $\eta_0 = 1^{\circ}$ down.

A comparison of the magnitudes of the pitch and yaw body rates for three initial angles of attack (0°, 1° up, and 5° up) is shown in figure 10. The "up" cases are presented because they generally resulted in larger angles of attack than the "down" cases, and, since the rates were to some extent dependent upon the magnitudes of the angles of attack, the rates also were larger. At the time these data were prepared, the 5°-up data were still available. From the data in figure 10, the similarity of the patterns for the various cases and the amplification of the magnitudes of the body rates by increasing the initial angle of attack are readily apparent. This effect on the magnitudes of the body rates is similar to the effect on the magnitudes of the angles of attack. (See fig. 9.) Up to about 140 seconds, both are increased as the initial angle of attack is increased. After 140 seconds, the magnitudes of both the angles of attack and the pitch and yaw body rates are uniformly high for all three initial angles of attack.

Effect of moments of inertia and rate of spin.- During the design phase of Project Fire, it was necessary to determine whether variations in the arrangement of the components and the consequent changes in the moments of inertia would appreciably affect the dynamic behavior of the vehicle during reentry, and thus become an important design factor. Consequently, trajectory computations were made in which the longitudinal and lateral moments of inertia were alternately increased and decreased by about 21 percent, with the spin rate remaining the same. The angle-of-attack variations for these trajectories are presented in figure 11.

The effect of changes in the rate of spin on the dynamic behavior was of interest in order to evaluate whether malfunction of the spin rockets by producing too little or too

much spin would be of serious consequence. Therefore, some computations were made in which the spin rates were increased and decreased by about 50 percent from the basic-case value. The results of these computations are shown in figure 12.

These two variables are discussed together because changes in the moment of inertia about the longitudinal axis (I_X) and in the spin rate about the same axis (p) do not directly affect the behavior; the effect of these variables is introduced through the change they make in the angular momentum term $(I_X p)$. A larger angular momentum, resulting from increased I_X or p, stiffens the vehicle's response to the pitching moment, and consequently the vehicle takes longer and goes to a higher angle of attack before the precessional motion starts. In the case of a smaller angular momentum, resulting from decreased I_X or p, the vehicle responds sooner and at a lower angle of attack. This increase or decrease in angle of attack is maintained through the entire trajectory. A comparison of the data presented in figures 11 and 12 shows that the changes in spin rate, which were relatively larger than the moment-of-inertia changes, had a greater effect on the angle-of-attack variations, as was expected. The run with zero spin rate is essentially a planar-oscillation trajectory, and the effect of spin on the response to the pitching moment is readily apparent.

Changes in the transverse moment of inertia (I_Y) comparable to changes in I_X affected the angle-of-attack variation only about half as much and in an opposite manner.

Effect of aerodynamic damping-moment coefficient.- The effect of increasing and decreasing the damping-moment coefficient is shown in figure 13. Although the general pattern for the angle-of-attack variation is similar for all these runs, the beneficial effect of increased aerodynamic damping is readily apparent in the delay of the angle-of-attack increase and the smaller final angle. Decreasing the aerodynamic damping, of course, had a corresponding adverse effect.

Results Obtained With Revised Program

The revised program was used to compute the effects of the static-stability coefficient and the Magnus moment coefficient. In addition, it was used to evaluate the angle-of-attack disturbances resulting from the tipoff moment, the imposed moment caused by asymmetric spring forces acting during separation of the velocity package from the reentry vehicle. The velocity package is the booster rocket used to increase the velocity of the vehicle to 37 000 ft/sec (11 278 m/sec) just prior to reentry. The effect of displacement of the center of gravity laterally from the axis of symmetry on the angle-of-attack variation also was determined with the new program.

Effect of static-stability coefficient.- Some computations were made to insure that reasonable variations in the static-stability coefficient C_{m_η} would not seriously affect

the dynamic behavior of the vehicle. Therefore, runs were made with C_{m_η} magnitudes of one-half and twice the basic-case value.

The effect of the changes in C_{m_η} on the angle-of-attack variation is shown in figure 14. Only the first 50 seconds of the flight are shown; however, the pattern suggests that the results for the remainder of the flights would be similar to the results for the spin-rate effect shown in figure 12. Increasing the value of C_{m_η} caused the vehicle to respond to the aerodynamic pitching moment sooner and at a somewhat smaller maximum angle of attack than in the basic case, similar to the behavior for decreased spin rate. This smaller angle of attack prevailed throughout the flight. A decrease in C_{m_η} had just the opposite effect.

The effect of changing C_{m_η} on the frequency of the precessional motion is shown in figure 15. An increase in C_{m_η} resulted in an increase in the precessional rate throughout the flight, compared with the basic case, in a manner similar to the way in which an increased spring constant causes an increased oscillation frequency. A decrease in C_{m_η} similarly reduced the precessional rate. The patterns, however, remained similar to the basic-case pattern.

Effect of tipoff moment.- Computations were made to investigate the effect of tipoff moments, moments that are induced by uneven spring forces acting during separation of the reentry vehicle from the velocity package. These tipoff moments were simulated by starting the computations essentially at $t = -1$ second and imposing a constant pitching moment about the body axis of 0.1 ft-lb (0.136 N-m), 0.2 ft-lb (0.271 N-m), and 1.0 ft-lb (1.356 N-m) for 1 second. Thus, at $t = 0$ and $h = 400\,000$ feet (122 000 meters), the perturbative effects of the tipoff moments are included. The data for these runs are shown in figure 16.

The patterns of the angle-of-attack variations with time are generally similar to results already discussed; however, the imposed tipoff moment induced a circular precessional motion before the vehicle entered the atmosphere. The rate of this precession is about 4 cps. The subsequent aerodynamic moment caused a more complicated epicyclic type of motion, in which the original circular precession became a sort of perturbation superimposed on a slower and larger precession. This motion is shown in figure 17. At the time equal to about 20 seconds, the basic precession has a rate of slightly less than 1/2 cps, and the superimposed perturbation has a rate of slightly more than 4 cps. (Actually, the ratio is about 9 to 1.) The magnitude of this perturbation is relatively large (about 60 percent of the magnitude of the basic motion). As the trajectory progresses through maximum dynamic pressure, the motion generally follows the already-established pattern in which the magnitude of the motion decreases to a minimum near peak dynamic pressure and then expands after this point, and the frequency of the motion peaks near maximum dynamic pressure. This pattern is shown in the following table:

Time, sec	Magnitude of angle-of-attack motion, deg		Frequency of angle-of-attack motion, cps	
	Basic motion	Perturbation	Basic motion	Perturbation
21.0	0.70	0.41	0.5	4.0
30.8	.56	.28	2.7	5.5
43.8	1.30	.28	1.2	4.9

These data show that the aerodynamic moment exerts a considerable influence on the magnitude and frequency of the basic precession, but only a minor influence on the perturbation. This is a normal development because the basic precession is a result of the spin and aerodynamic moment, whereas the perturbation is a result of the spin and the independently applied tipoff moment.

Effect of center-of-gravity displacement.- For these computations the center of gravity was assumed to be laterally off the axis of symmetry by 0.01, 0.03, and 0.06 foot (0.003, 0.009, and 0.018 meter). The data for these tests are presented in figure 18. The fact that the center of gravity is no longer on the axis of symmetry means that the aerodynamic axial-force component, which acts along the axis of symmetry, will introduce a transverse disturbing moment about the body axis throughout the flight. During the early portion of the runs (less than 50 seconds), the effect of the asymmetry was large, causing the magnitude of the angle of attack to increase from less than 1^{o} up to about 4^{o}, 14^{o}, and 28^{o} for displacements of 0.01, 0.03, and 0.06 foot (0.003, 0.009, and 0.018 meter). The peaks in the angle-of-attack curves occur at about the time of maximum dynamic pressure (about 30 seconds) because the main disturbing force, the drag, also is maximum here. At the later times, above about 110 seconds, increasing the center-of-gravity displacement resulted mainly in broadening the angle-of-attack envelope.

The pitch-yaw motion during three time periods is shown in figure 19 for the 0.03-foot (0.009-meter) center-of-gravity displacement. This motion is representative of the motion for the other center-of-gravity displacements; only the magnitudes differ. The first two time periods show the gradual buildup of the motion to about the maximum values. The third plot shows the irregular motion that develops. From the data in this plot, it is apparent why the spread of the angle-of-attack limits becomes so large.

Effect of Magnus moment coefficient.- A spinning vehicle traveling through an atmosphere will generate a Magnus force and moment if it is at an angle of attack other than zero. The Project Fire reentry vehicle spins rather rapidly; therefore, investigation of these Magnus effects seemed desirable. Actually, the Magnus forces do not affect the stability directly, but the integration of the forces along the body produces a moment

about the center of gravity that affects the stability. Therefore, an aerodynamic Magnus moment coefficient $(C_n)_{p,\eta}$ that was considered reasonable for the short vehicle was introduced into the equations of motion. In figure 20 it can be seen that a Magnus moment coefficient of this magnitude $\left((C_n)_{p,\eta} = 0.000175 \text{ per deg}\right)$ produced only a negligible effect on the dynamic behavior of the vehicle.

CONCLUDING REMARKS

An analytical investigation has been made of the effects of various physical and aerodynamic parameters on the dynamic behavior of the Project Fire reentry vehicle during its reentry. Since the vehicle was designed to spin at a high rate (3 rps), a 5-degree-of-freedom set of equations was used with the spin rate specified constant. For the computations, the mass and aerodynamic characteristics remained constant throughout a run.

The results of the investigation showed that for most of the aerodynamic and physical parameters considered, a reasonable change from the basic-case value did not seriously alter the angle-of-attack variation; that is, the angles of attack remained small (about 5°) during the main heating period (the initial 40 seconds) and thus were below values that would compromise the mission. Of the variables tested, only mass asymmetry produced large disturbances. When the center of gravity was displaced from the axis of symmetry by about 1/8 inch (0.003 meter), the magnitude of the angle of attack approached 5° during the early part of the run. The results also showed that the deceleration along the flight path would be high (about 75g at the peak) and that the vehicle motion would produce quite high angular rates about the body axes, varying between the limits of ±200 deg/sec.

Langley Research Center,
National Aeronautics and Space Administration,
Langley Station, Hampton, Va., January 23, 1968,
714-00-00-01-23.

APPENDIX

EQUATIONS OF MOTION

The equations of motion used in this investigation are for a modified body-axis system. (See fig. 1.) This system differs from the usual body-axis system in that the Z-axis is constrained to remain in a plane parallel to the X_iZ_i-plane and in that the body is free to spin about the X body axis, which results in there being no X-moment equation. The X-axis is always alined with the axis of symmetry of the body. The equations are in a form frequently employed in ballistics work, and they may be derived by resolving equations of motion in a standard body-axis system into the modified body-axis system as shown in reference 1. Therefore, a full development of the equations will not be presented. The equations used herein are as follows:

X-force equation:

$$\dot{u} = \frac{q_p A}{m} C_X \cos \eta + rv - qw - g \frac{r_e^2}{r^3}(x \cos \psi \cos \theta + y \sin \theta + z \sin \psi \cos \theta)$$

Y-force equation:

$$\dot{v} = \frac{q_p A}{m}\left(C_{Y_\eta} \frac{v}{V_a} + C_{Yb} \cos \phi - C_{Zb} \sin \phi\right) - ru + qw \tan \theta$$

$$- g \frac{r_e^2}{r^3}(-x \cos \psi \sin \theta + y \cos \theta - z \sin \psi \sin \theta)$$

Z-force equation:

$$\dot{w} = \frac{q_p A}{m}\left(C_{Z_\eta} \frac{w}{V_a} + C_{Yb} \sin \phi + C_{Zb} \cos \phi\right) + qu - qv \tan \theta$$

$$- g \frac{r_e^2}{r^3}(-x \sin \psi + z \cos \psi)$$

Y-moment equation:

$$\dot{q} = \frac{q_p A d}{I_Y}\left(C_{m_\eta} \frac{w}{V_a} + C_X \frac{l}{d} \sin \phi + (C_m)_{p,\eta} \frac{pd}{2V_a} \frac{v}{V_a} + C_{m_q} \frac{qd}{2V_a}\right)$$

$$+ \frac{1}{I_Y}\left(M_{Yb} \cos \phi - M_{Zb} \sin \phi\right) - \frac{I_X}{I_Y} pr + rq \tan \theta$$

APPENDIX

Z-moment equation:

$$\dot{r} = \frac{q_p A d}{I_Z}\left(C_{n_\eta}\frac{v}{V_a} - C_X\frac{l}{d}\cos\phi + (C_n)_{p,\eta}\frac{pd}{2V_a}\frac{w}{V_a} + C_{n_r}\frac{rd}{2V_a}\right)$$

$$+\frac{1}{I_Z}\left(M_{Zb}\cos\phi + M_{Yb}\sin\phi\right) + \frac{I_X}{I_Y}pq - q^2\tan\theta$$

where

$$\dot{\phi} = p - q\tan\theta$$

$$\dot{\theta} = r$$

$$\dot{\psi} = -\frac{q}{\cos\theta}$$

$$\dot{x} = u\cos\theta\cos\psi - v\sin\theta\cos\psi - w\sin\psi$$

$$\dot{y} = u\sin\theta + v\cos\theta$$

$$\dot{z} = u\cos\theta\sin\psi - v\sin\theta\sin\psi + w\cos\psi$$

$$\eta = \sin^{-1}\frac{\sqrt{v^2 + w^2}}{V_a}$$

$$V_a = \sqrt{u^2 + v^2 + w^2}$$

$$A_{V_a} = \frac{\Delta V_a}{\Delta t}\times\frac{1}{g}$$

$$r = \sqrt{x_i^2 + y_i^2 + z_i^2}$$

$$h = r - r_e$$

$$\rho = f(h)$$

The 1959 ARDC atmosphere was used for ρ. (See ref. 2.) The body angular rates were:

$$p_b = p$$

$$q_b = q\cos\phi + r\sin\phi$$

$$r_b = r\cos\phi - q\sin\phi$$

The terms M_{Yb} and M_{Zb} are arbitrary body moments and were programed as functions of time to simulate the tipoff-moment effects.

REFERENCES

1. Bird, John D.; and Llewellyn, Charles P.: An Analysis of the Stability of Spinning Disks During Atmospheric Reentry. NASA TM X-248, 1960.

2. Minzner, R. A.; Champion, K. S. W.; and Pond, H. L.: The ARDC Model Atmosphere, 1959. Air Force Surv. in Geophys. No. 115 (AFCRC-TR-59-267), Air Force Cambridge Res. Center, Aug. 1959.

TABLE I.- PARAMETERS CONSTANT FOR ALL COMPUTATIONS

m	6.22 slugs (90.774 kg)
d	2.11 ft (0.643 m)
A	3.495 ft^2 (0.325 m^2)
C_X	-1.43
$C_{Y_\eta} = C_{Z_\eta}$	-0.23
γ_o	-14.7^o
$V_{i,o}$	37 000 ft/sec (11 278 m/sec)
h_o	400 000 ft (121 920 m)

TABLE II.- PARAMETERS USED IN THE ORIGINAL PROGRAM

$\left[C_{m_\eta} = -C_{n_\eta} = -0.08/\text{rad};\ (C_n)_{p,\eta} = 0;\ M_{YB} = 0;\ \text{c.g. displacement} = 0\right]$

Run no.	I_X,		$I_Y = I_Z$,		$C_{m_q} = C_{n_r}$	p, rad/sec	η_o, deg	ψ_o, deg
	slug-ft^2	kg-m^2	slug-ft^2	kg-m^2				
1 (Basic case)	2.8	3.80	2.3	3.12	-0.08	18.84	0	-14.7
2	3.4	4.61	2.3	3.12	-.08	18.84	0	-14.7
3	2.2	2.98	2.3	3.12	-.08	18.84	0	-14.7
4	2.8	3.80	2.8	3.80	-.08	18.84	0	-14.7
5	2.8	3.80	1.8	2.44	-.08	18.84	0	-14.7
6	2.8	3.80	2.3	3.12	-.08	18.84	1 up	-13.7
7	2.8	3.80	2.3	3.12	-.08	18.84	1 down	-15.7
8	2.8	3.80	2.3	3.12	-.08	18.84	5 down	-19.7
9	2.8	3.80	2.3	3.12	-.08	9.425	0	-14.7
10	2.8	3.80	2.3	3.12	-.08	29.531	0	-14.7
11	2.8	3.80	2.3	3.12	-.08	0	0	-14.7
12	2.8	3.80	2.3	3.12	-.44	18.84	0	-14.7
13	2.8	3.80	2.3	3.12	-1.0	18.84	0	-14.7
14	2.8	3.80	2.3	3.12	.0	18.84	0	-14.7
15	2.8	3.80	2.3	3.12	.2	18.84	0	-14.7

TABLE III.- PARAMETERS USED IN THE REVISED PROGRAM

[I_X = 2.8 slug-ft^2 (3.80 kg-m^2); $I_Y = I_Z$ = 2.3 slug-ft^2 (3.12 kg-m^2); $C_{m_q} = C_{n_r}$ = -0.08; p = 18.84 rad/sec; $\eta_o = 0^o$; $\psi_o = -14.7^o$]

Run no.	$C_{m_\eta} = -C_{n_\eta}$, per rad	$(C_n)_{p,\eta}$, per deg	M_{Yb},		c.g. displacement,	
			ft-lb	N-m	ft	m
16	-0.04	0	0	0	0	0
17	-.16	0	0	0	0	0
18	-.08	.000175	0	0	0	0
19	-.08	0	.1	.136	0	0
20	-.08	0	.2	.271	0	0
21	-.08	0	1.0	1.356	0	0
22	-.08	0	0	0	.01	.003
23	-.08	0	0	0	.03	.009
24	-.08	0	0	0	.06	.018

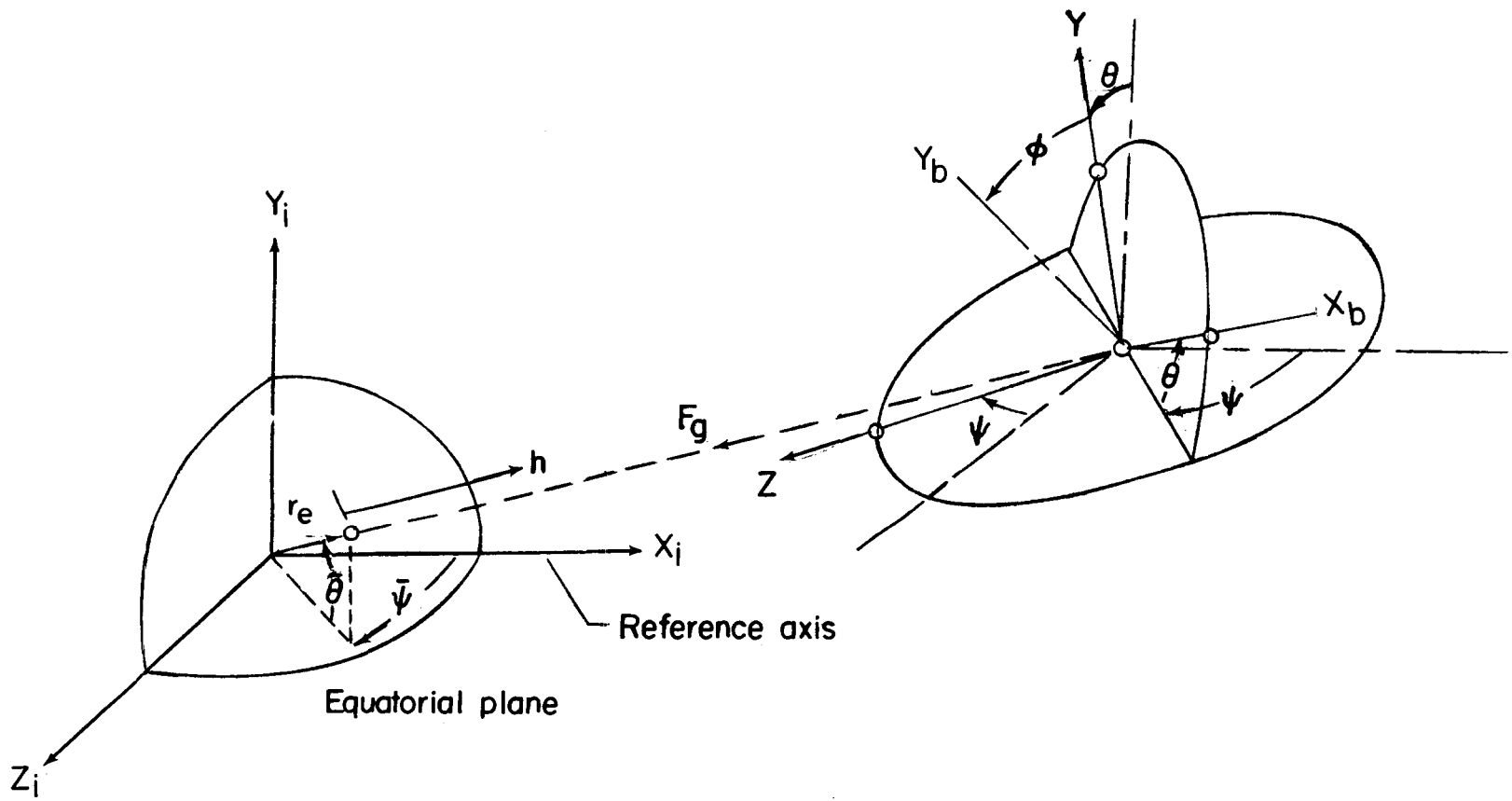

Figure 1.- Axis systems used in the analysis.

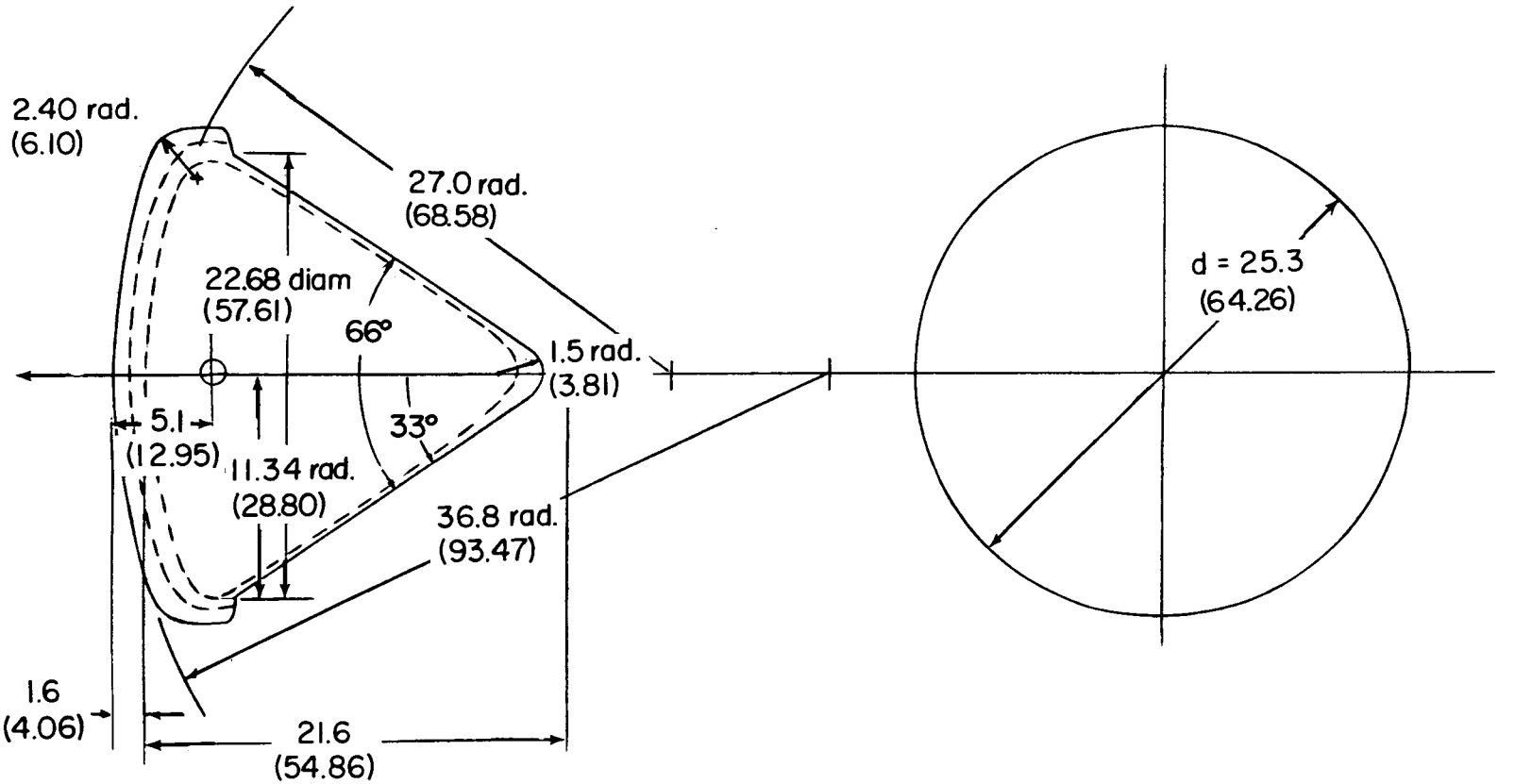

Figure 2.- Sketch of the Project Fire reentry vehicle. All dimensions are in inches and parenthetically in centimeters unless indicated otherwise.

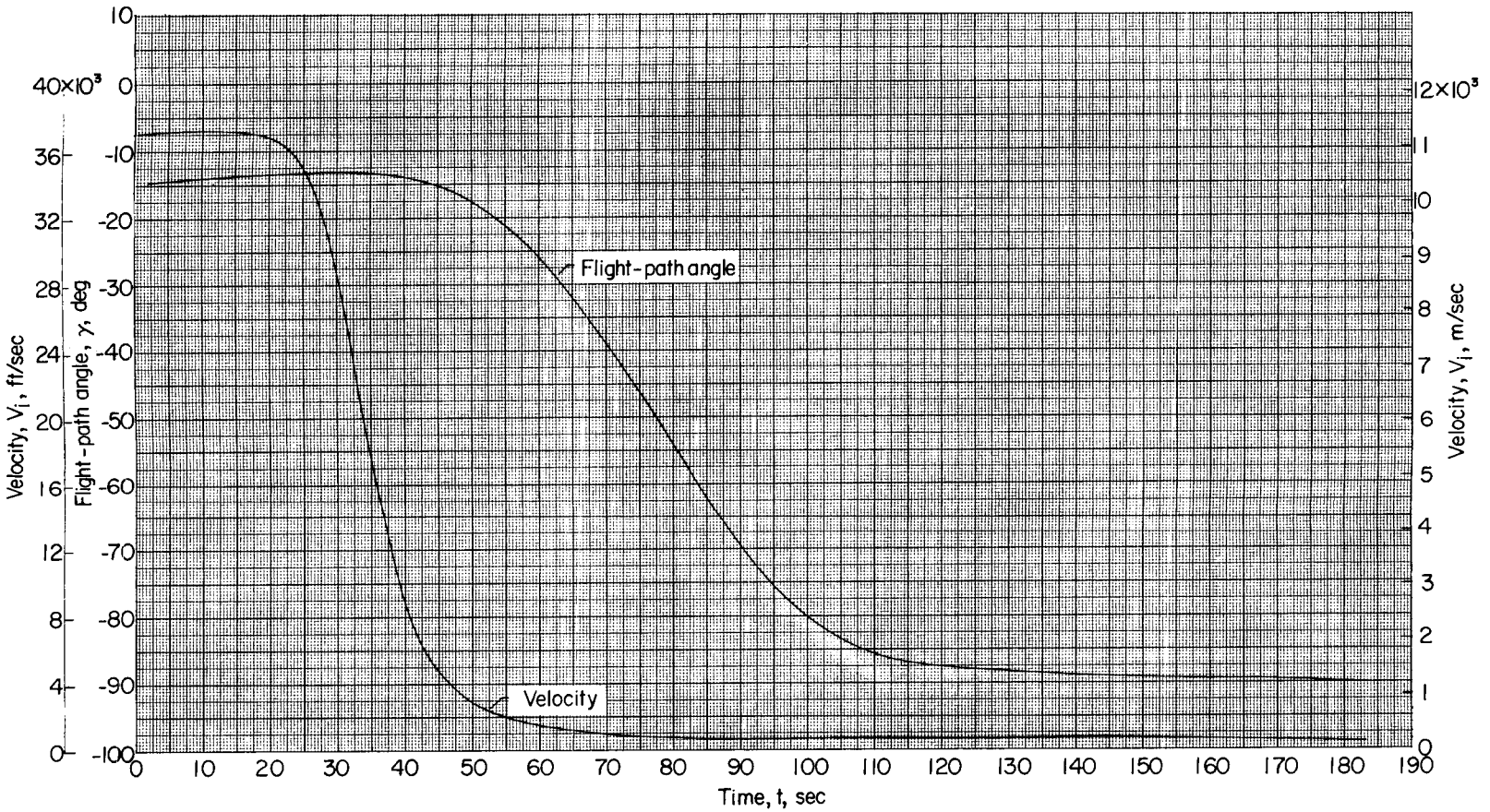

(a) Variation of velocity and flight-path angle.

Figure 3.- Variation of velocity, flight-path angle, altitude, range, deceleration, and dynamic pressure with time for the Project Fire reentry vehicle. (Basic case.)

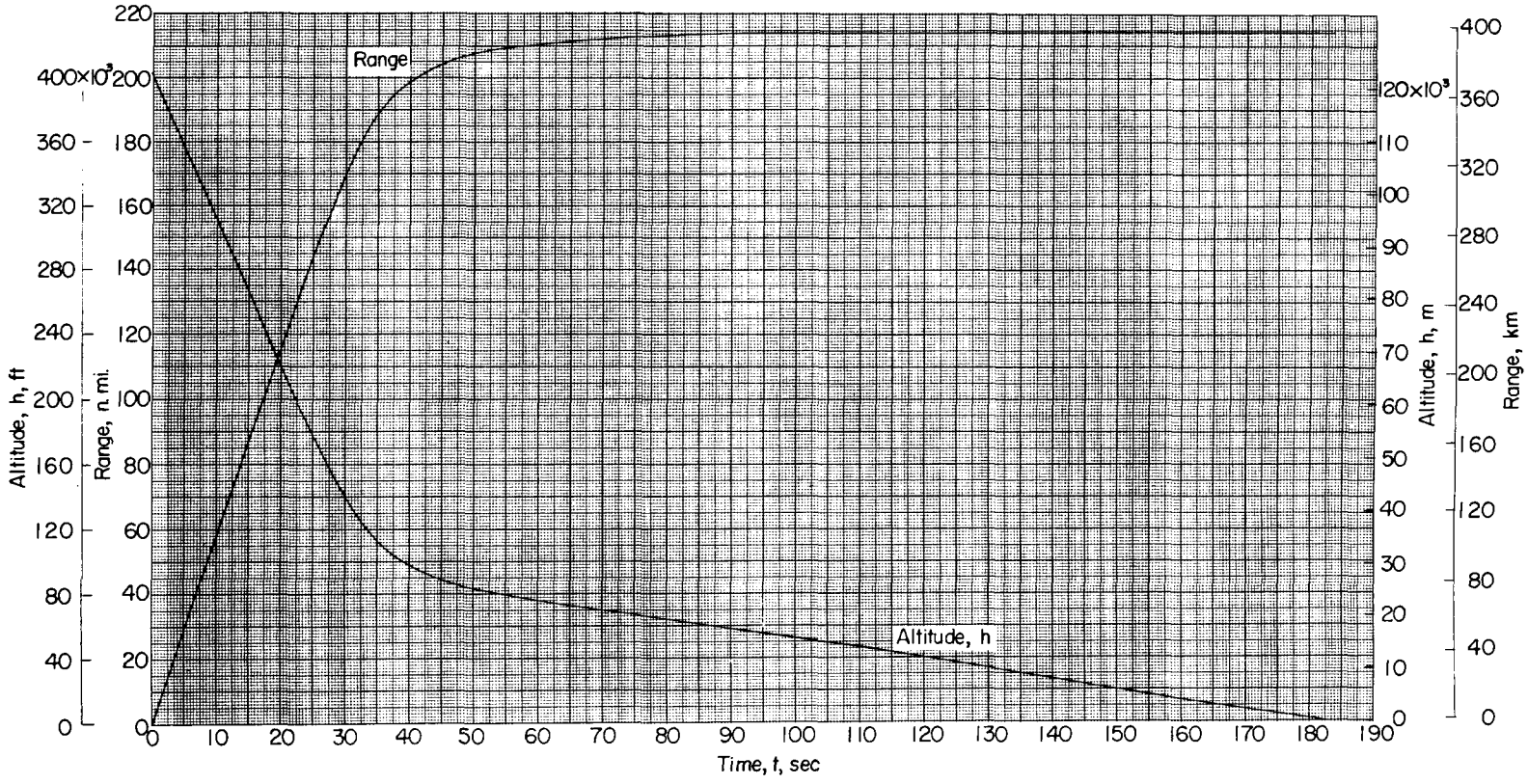

(b) Variation of altitude and range.

Figure 3.- Continued.

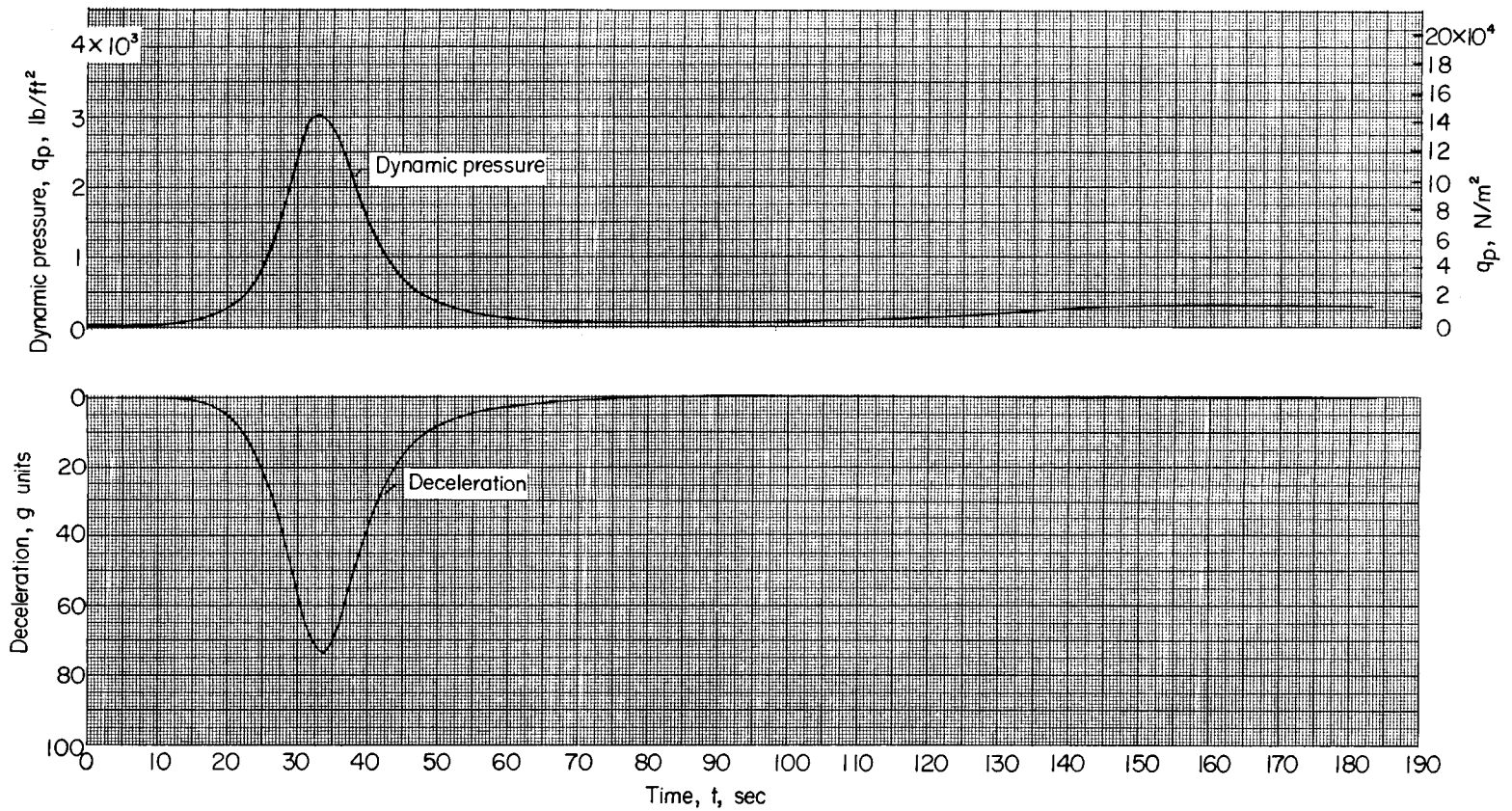

(c) Variation of deceleration and dynamic pressure.

Figure 3.- Concluded.

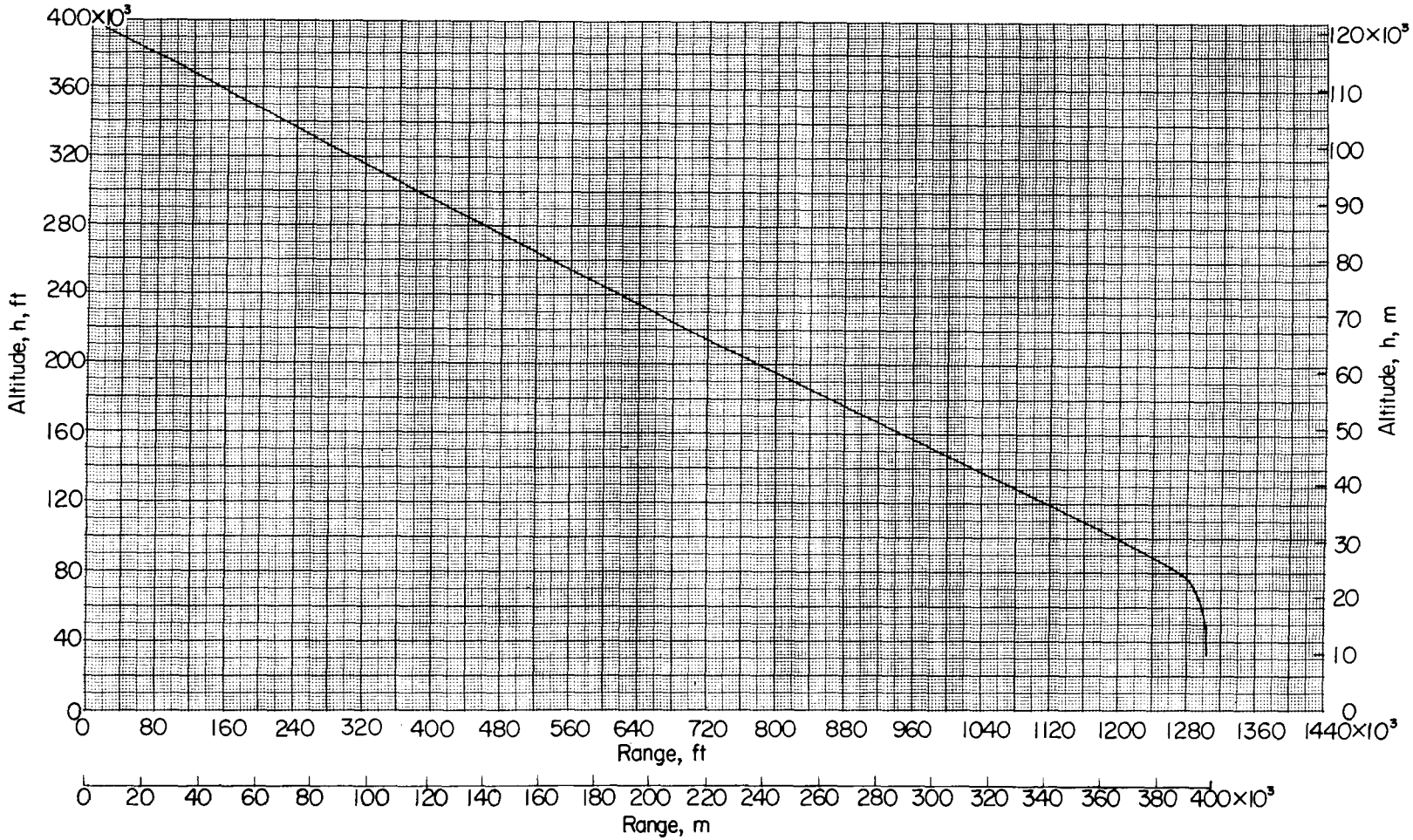

Figure 4.- Variation of altitude with range from entry for the Project Fire reentry vehicle. (Basic case.)

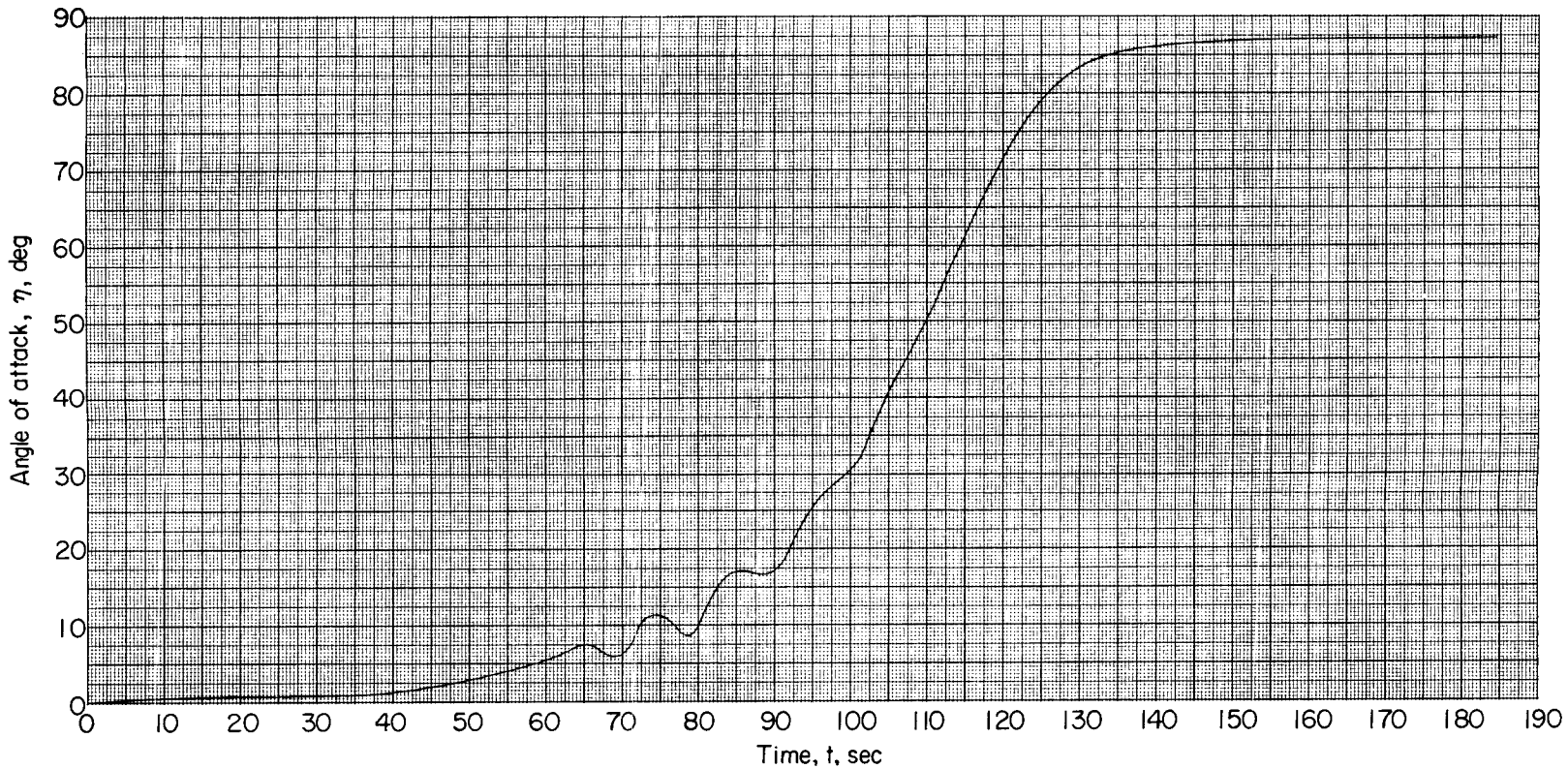

(a) Variation for the full reentry time.

Figure 5.- Variation of the angle of attack with time for the Project Fire reentry vehicle. (Basic case.)

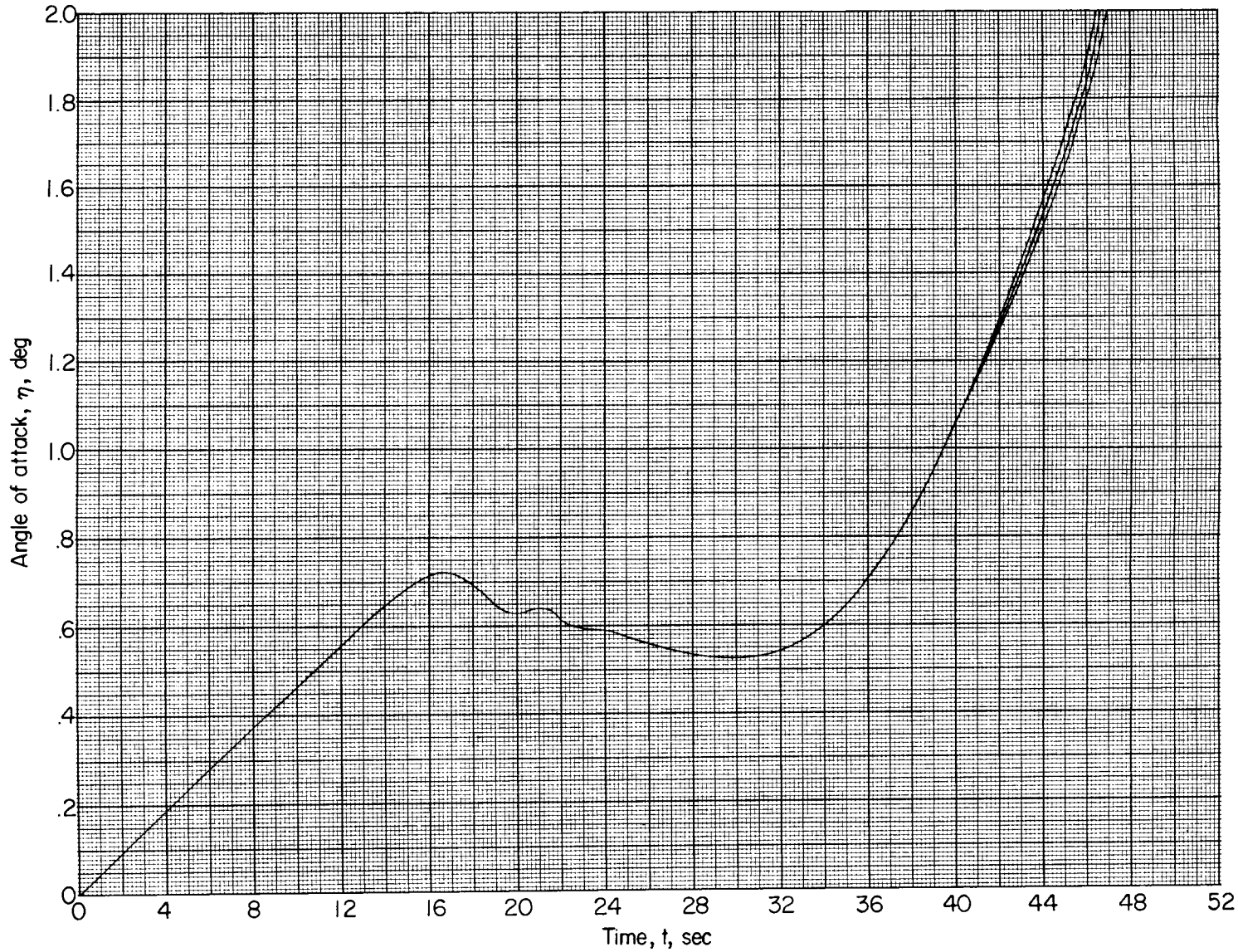

(b) Variation for the first 50 seconds of reentry. The triple lines indicate the angle-of-attack envelope and the mean values which will be used hereafter.

Figure 5.- Concluded.

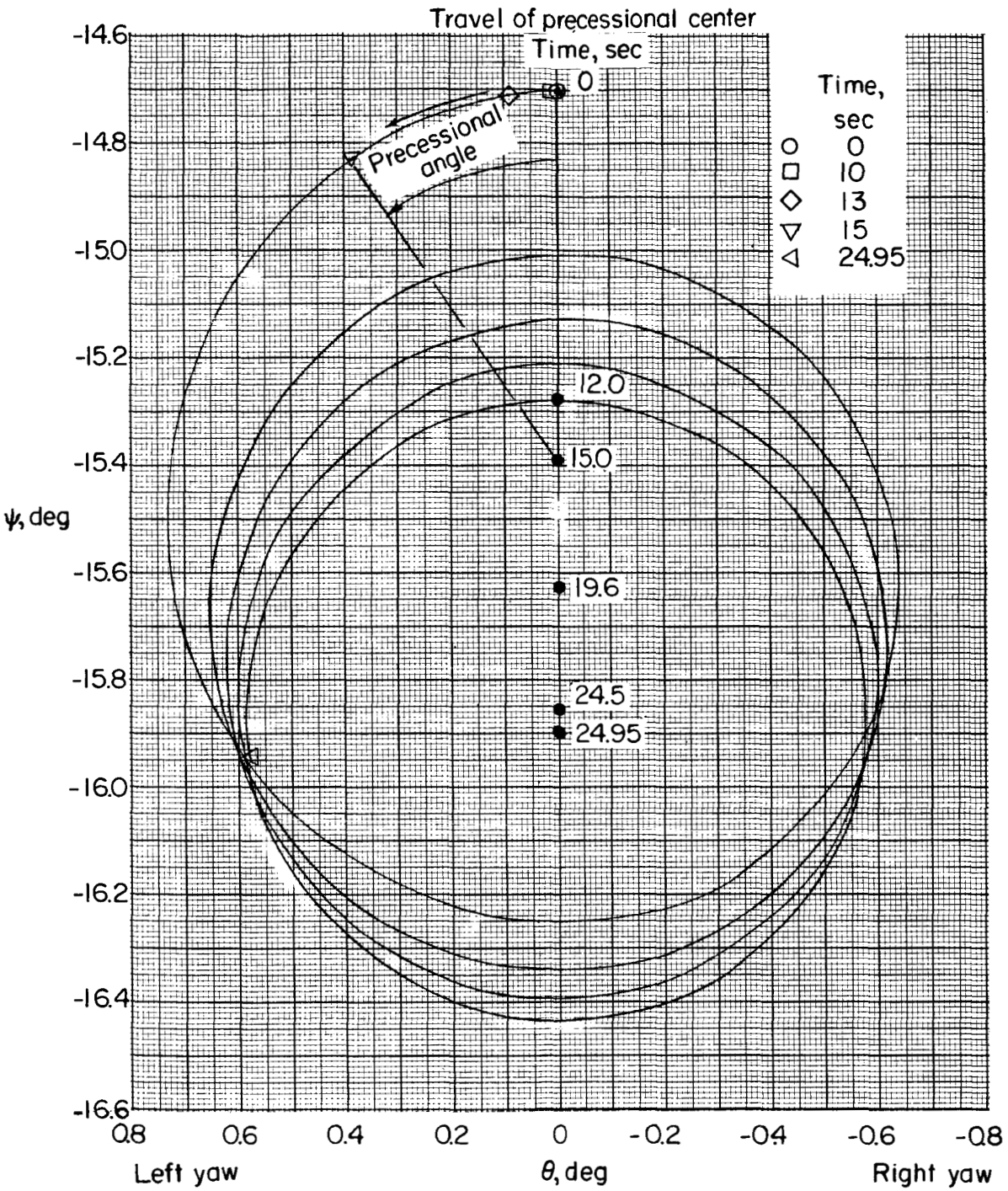

(a) Time from 0 to 24.95 seconds.

Figure 6.- Precessional motion of the Project Fire reentry vehicle during various time periods of the reentry. (Basic case.) The angle ψ is the pitch angle, measured from the horizontal at the initial entry point, and θ is the yaw angle. The declination of the instantaneous precessional center is shown by crosses along the $\theta = 0^0$ line.

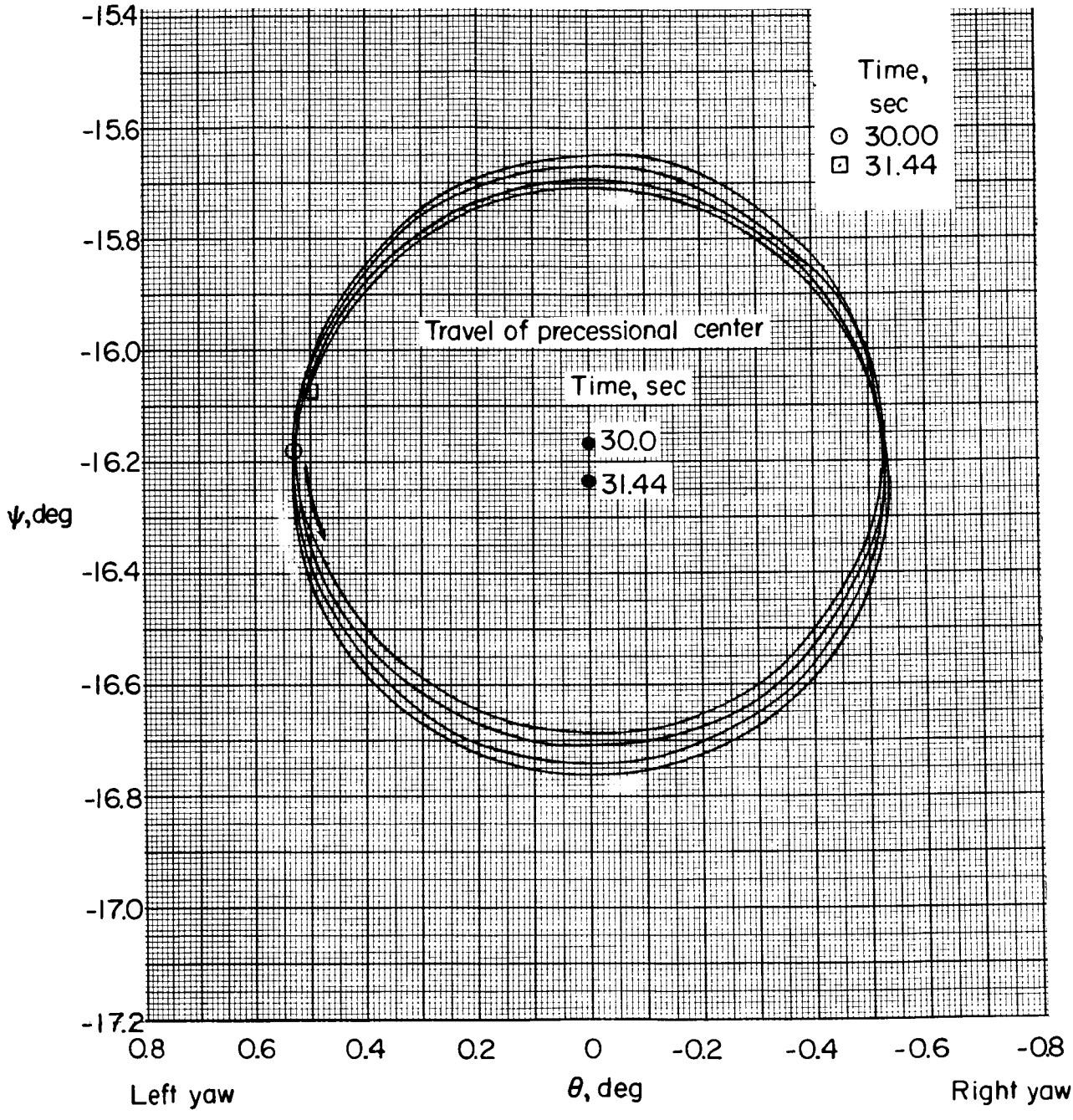

(b) Time from 30.00 to 31.44 seconds.

Figure 6.- Continued.

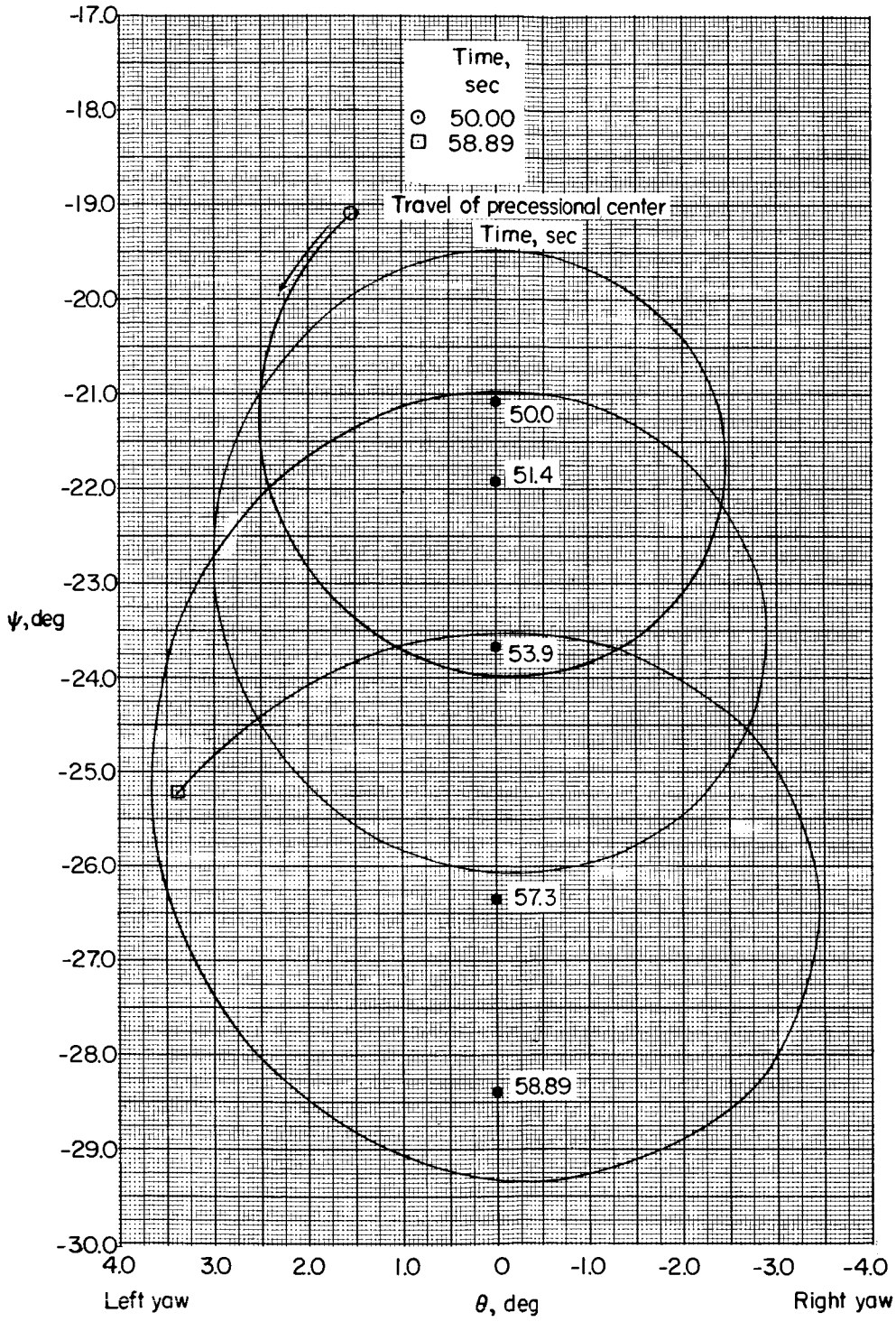

(c) Time from 50.00 to 58.89 seconds.

Figure 6.- Continued.

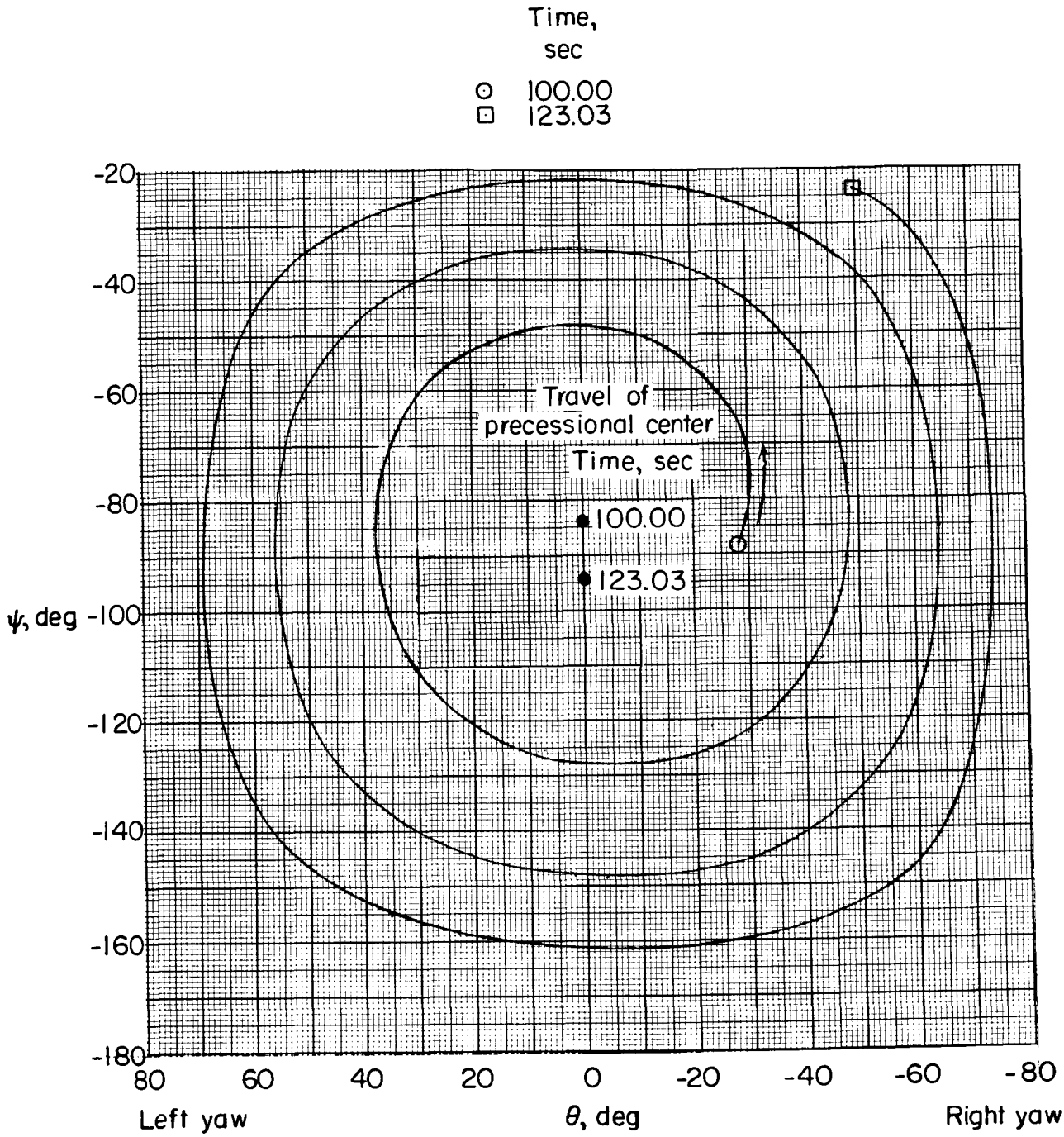

(d) Time from 100.00 to 123.03 seconds.

Figure 6.- Concluded.

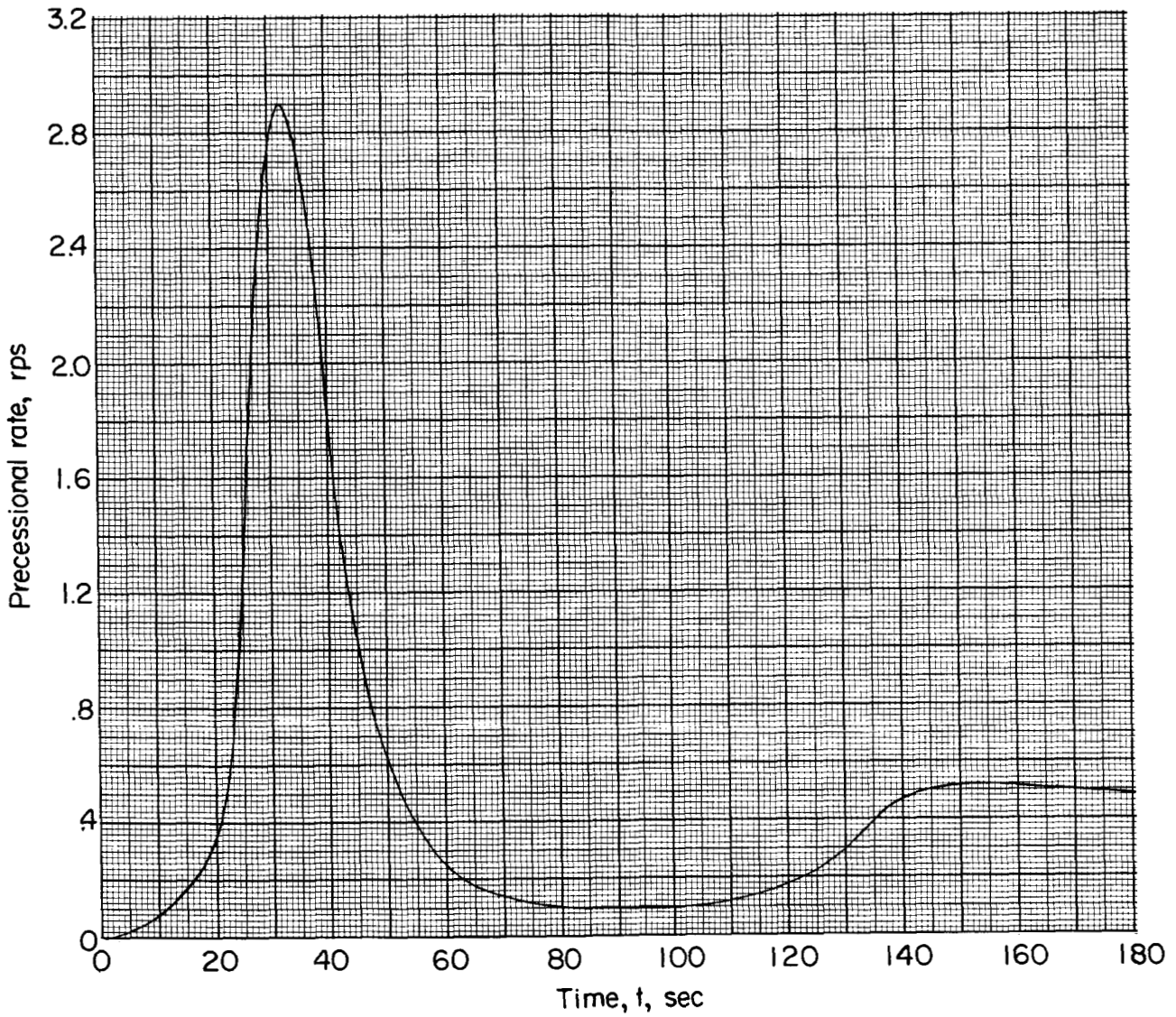

Figure 7.- Variation of precessional rate with time. (Basic case.)

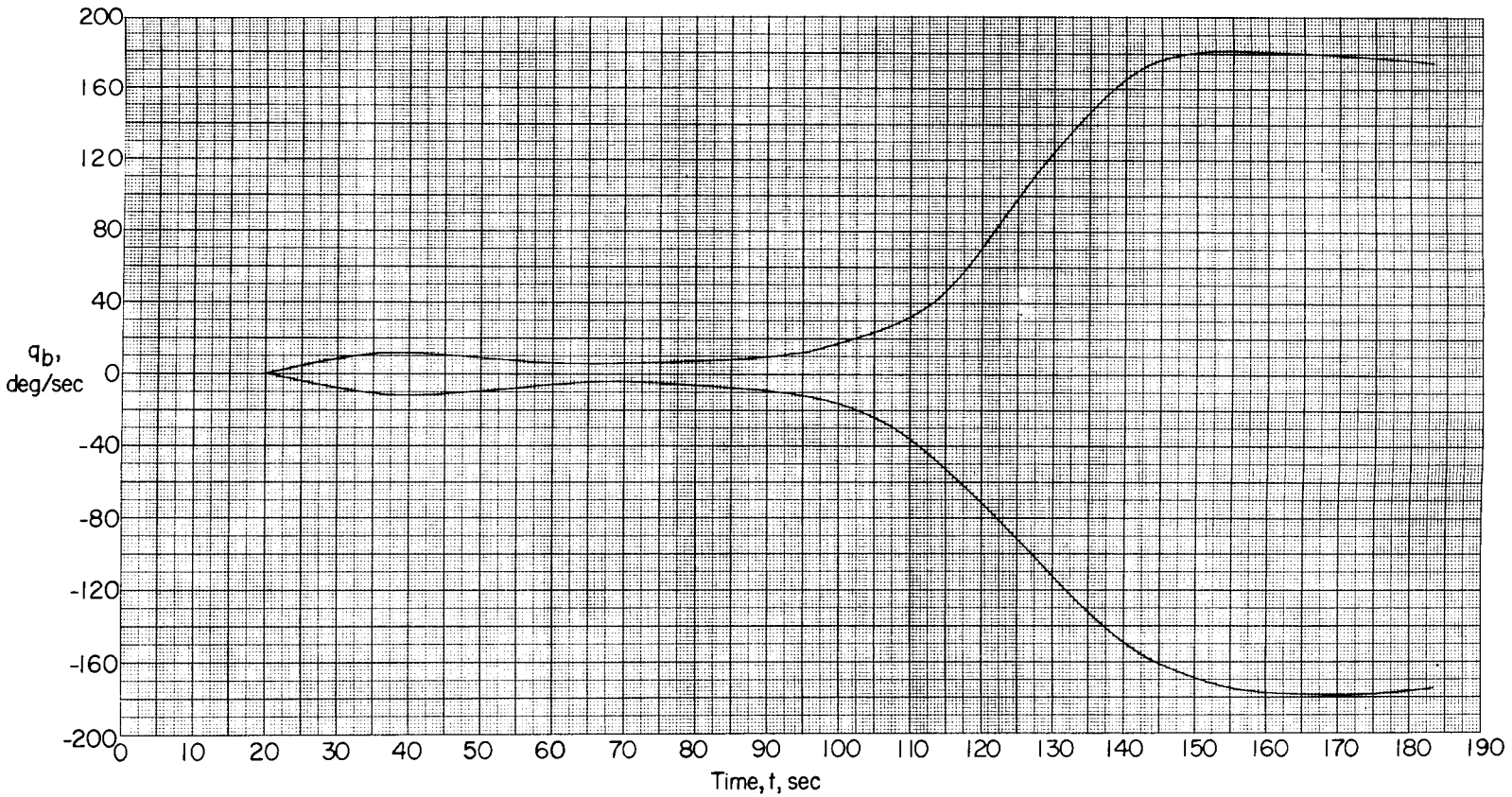

(a) Variation of pitch body rate.

Figure 8.- Variation of the envelopes of pitch and yaw body rates with time for the Project Fire reentry vehicle. (Base case.) The actual body rates oscillate between the envelope limits because of the spin rate.

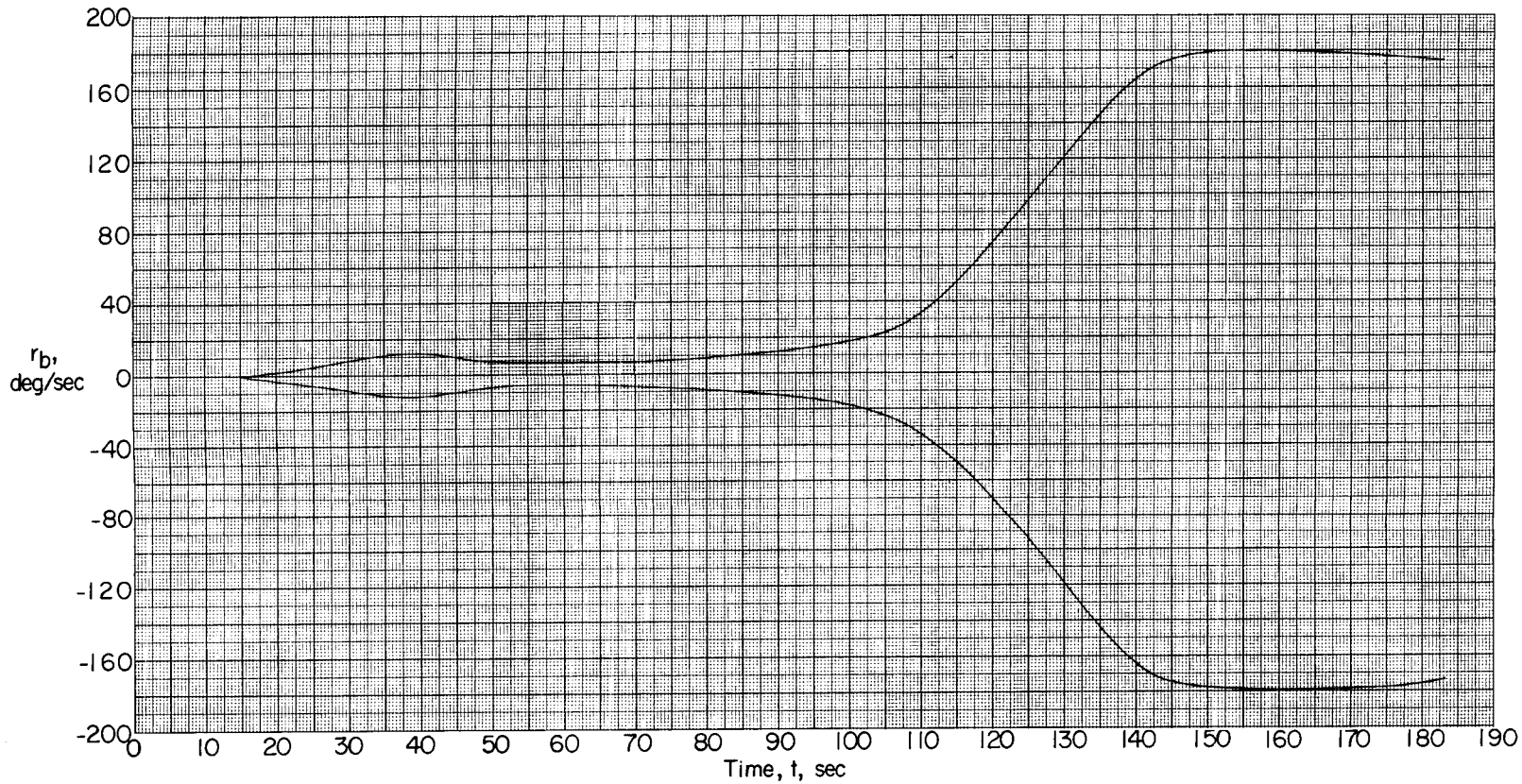

(b) Variation of yaw body rate.

Figure 8.- Concluded.

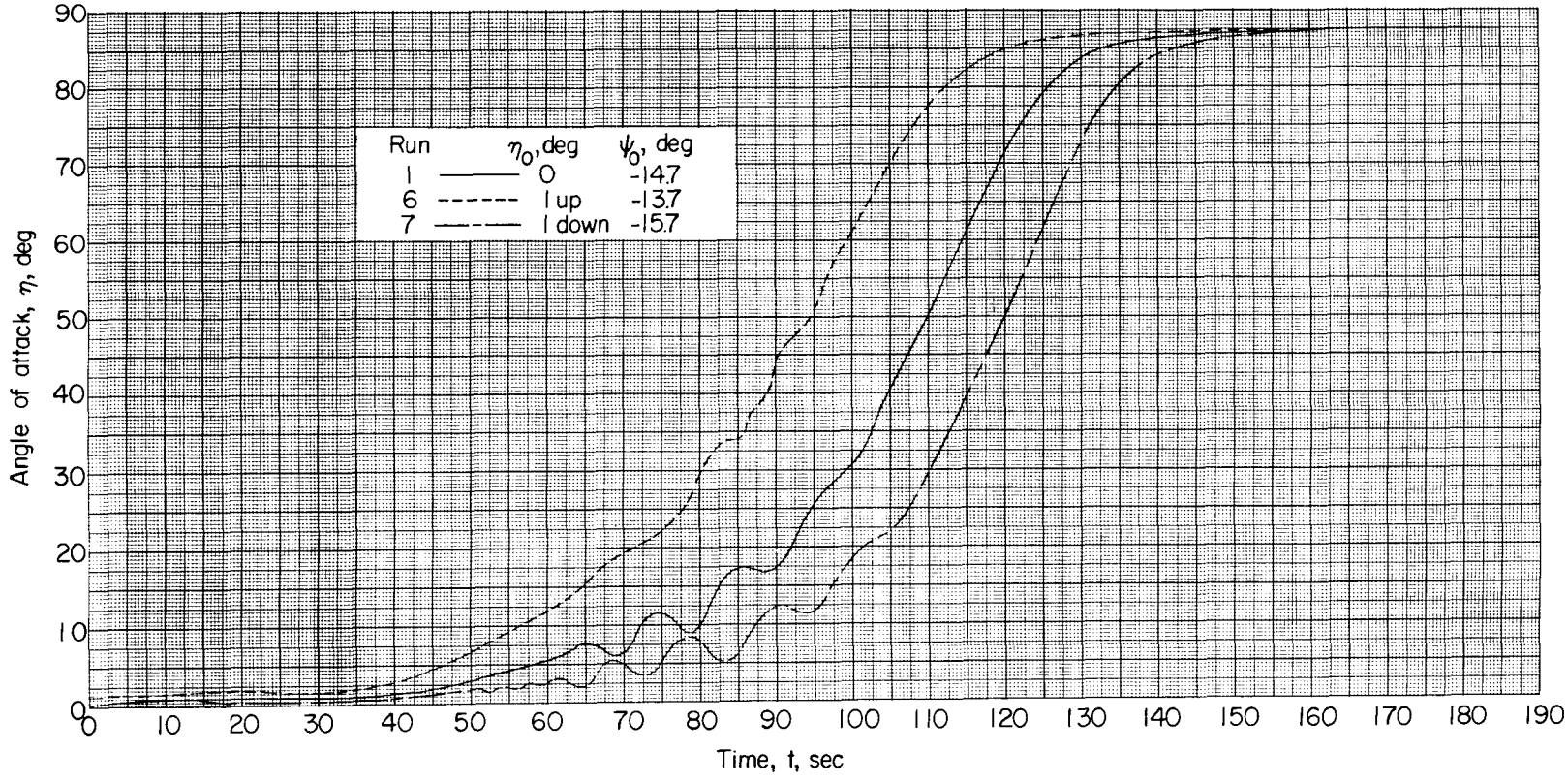

(a) Variation for the full reentry time for 1^0 initial angles of attack.

Figure 9.- Effect of initial pitch angle and initial angle of attack on the angle-of-attack variation with time for the Project Fire reentry vehicle. The run numbers correspond to those in tables II and III.

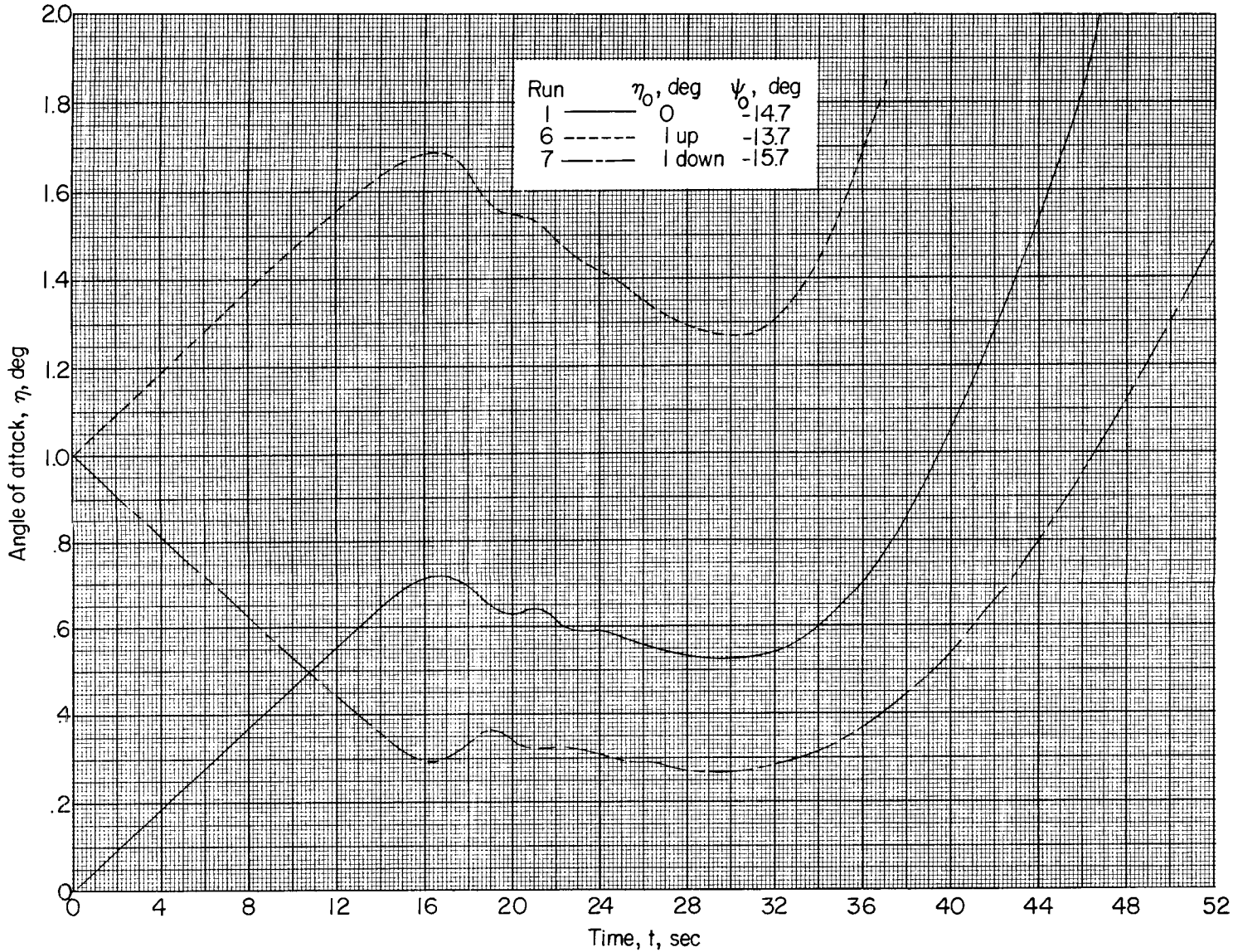

(b) Variation for the first 50 seconds of reentry for 1^0 initial angles of attack.

Figure 9.- Continued.

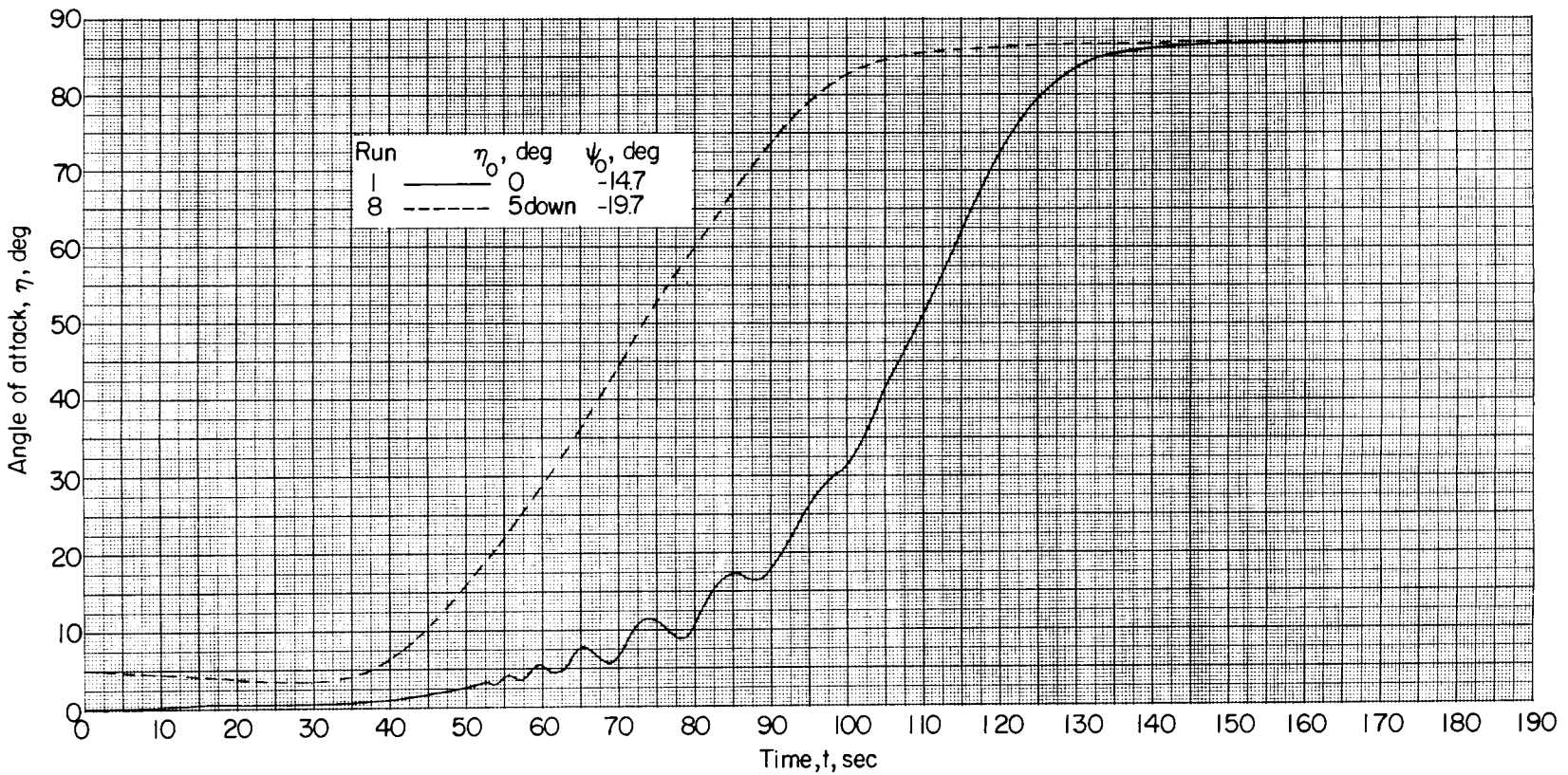

(c) Variation for the full reentry time for 5^0 initial angle of attack.

Figure 9.- Concluded.

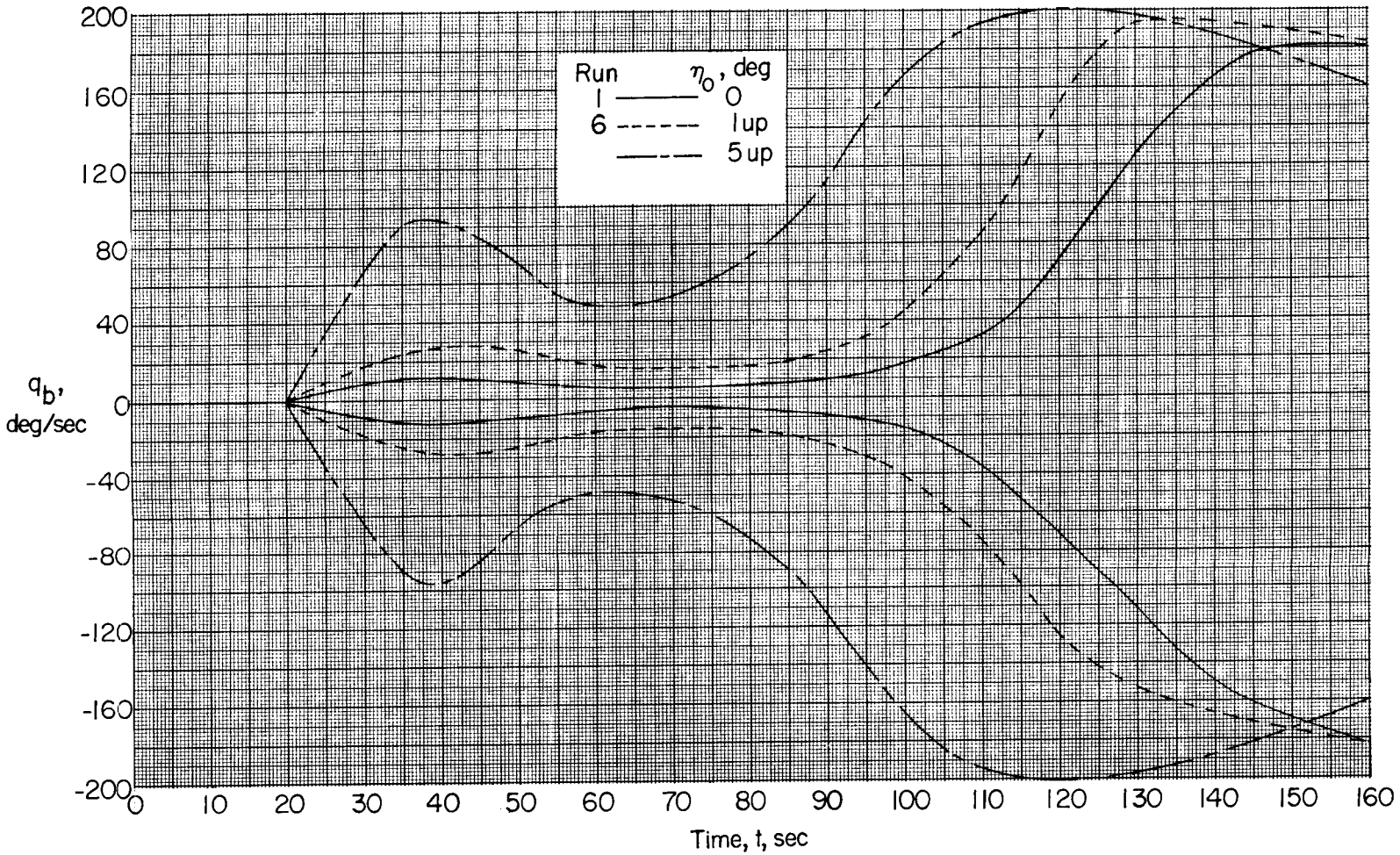

(a) Variation of pitch body rate.

Figure 10.- Variation of the envelopes of pitch and yaw body rates with time for three initial angles of attack of the Project Fire reentry vehicle. The actual body rates oscillate between the envelope limits because of the spin rate.

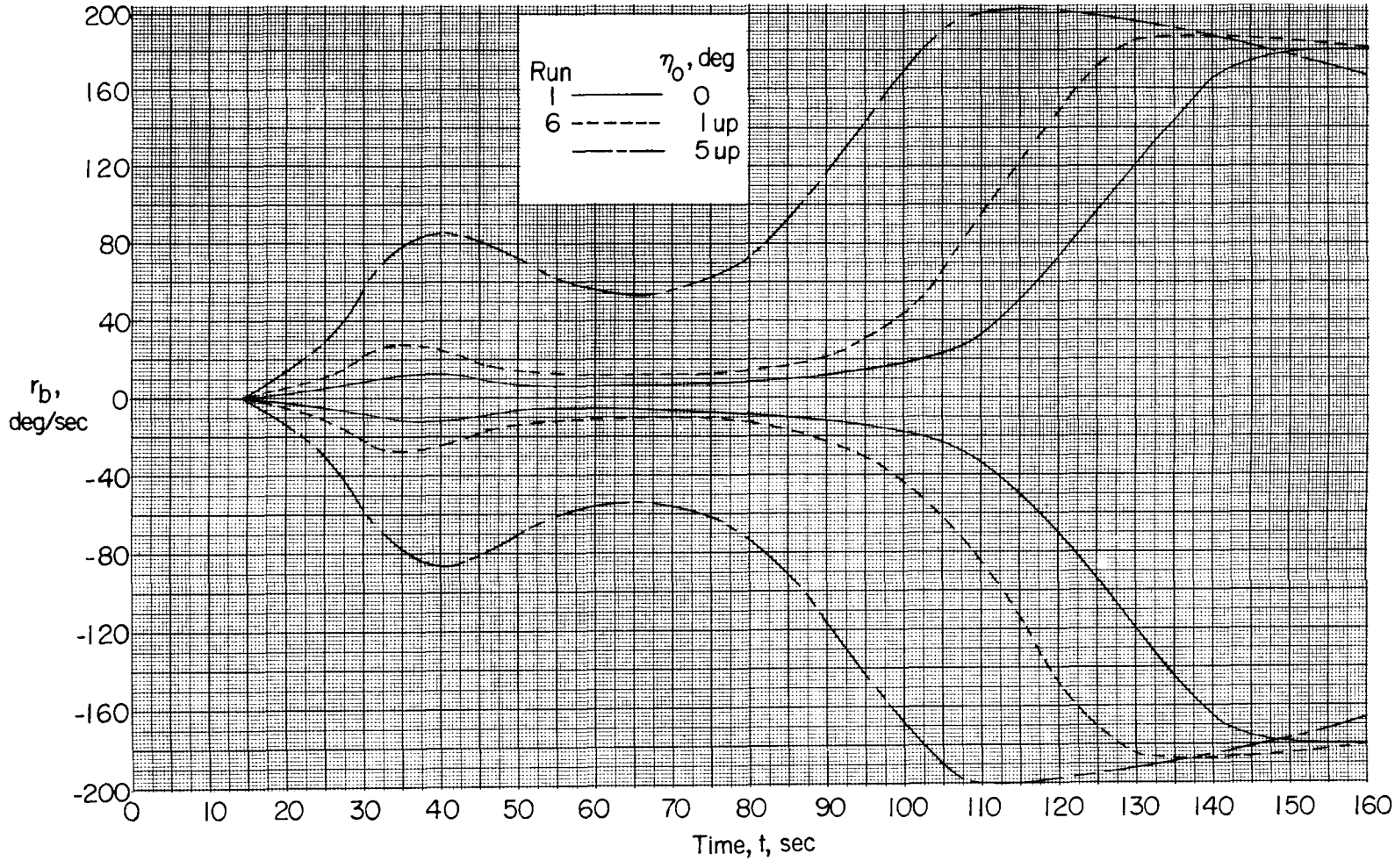

(b) Variation of yaw body rate.

Figure 10.- Concluded.

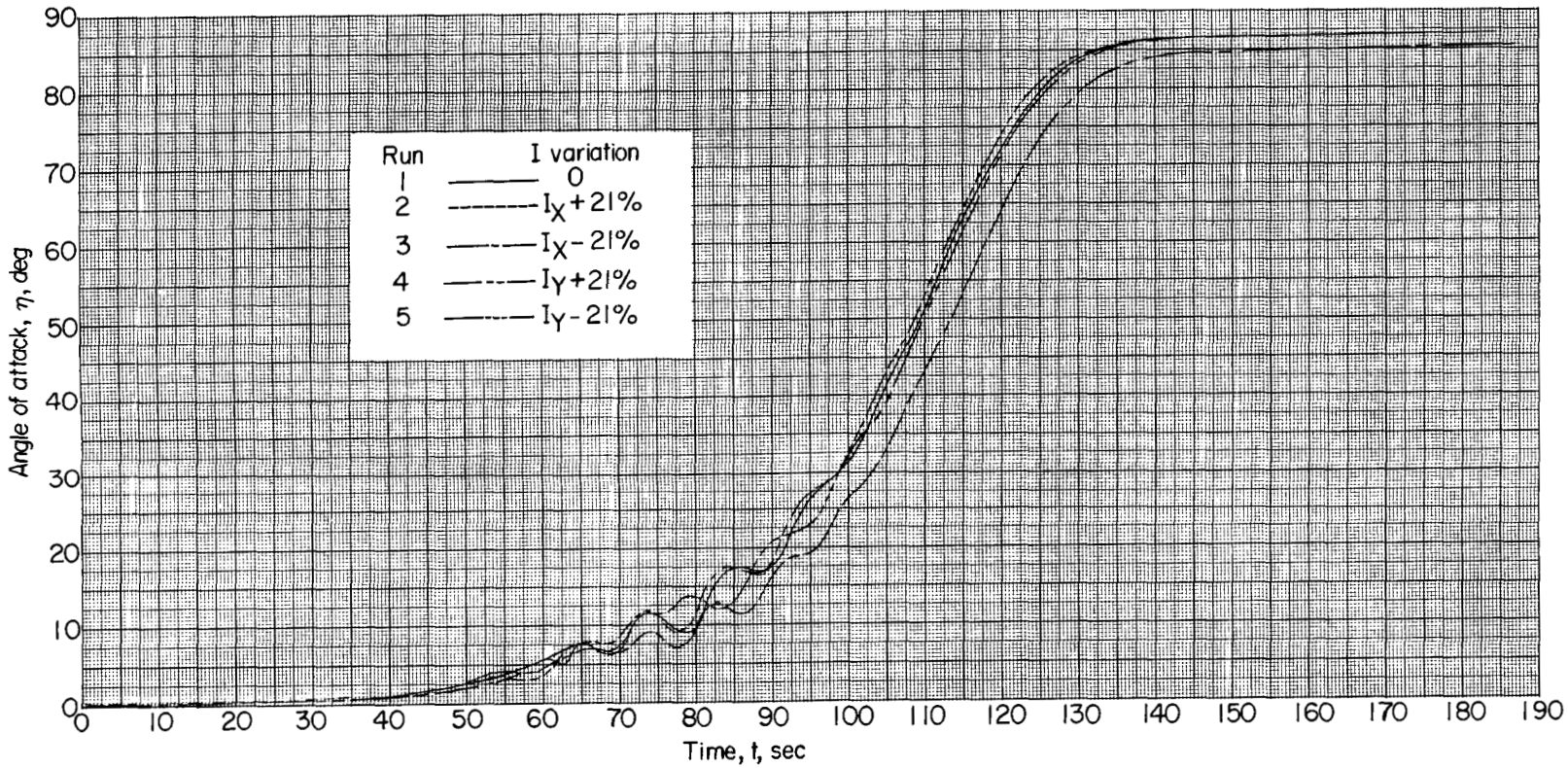

(a) Variation for the full reentry time.

Figure 11.- Effect of moment of inertia on the angle-of-attack variation with time for the Project Fire reentry vehicle.

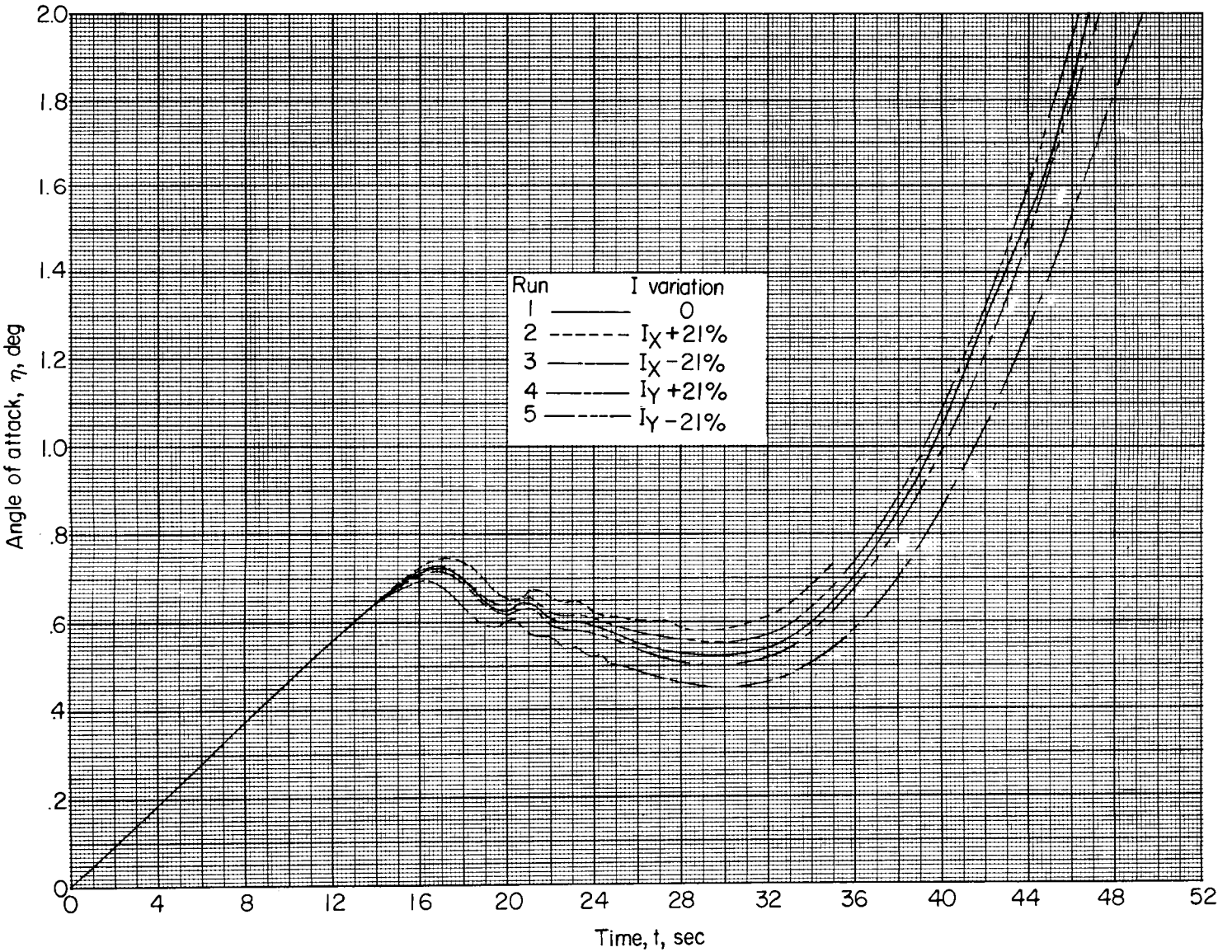

(b) Variation for the first 50 seconds of reentry.

Figure 11.- Concluded.

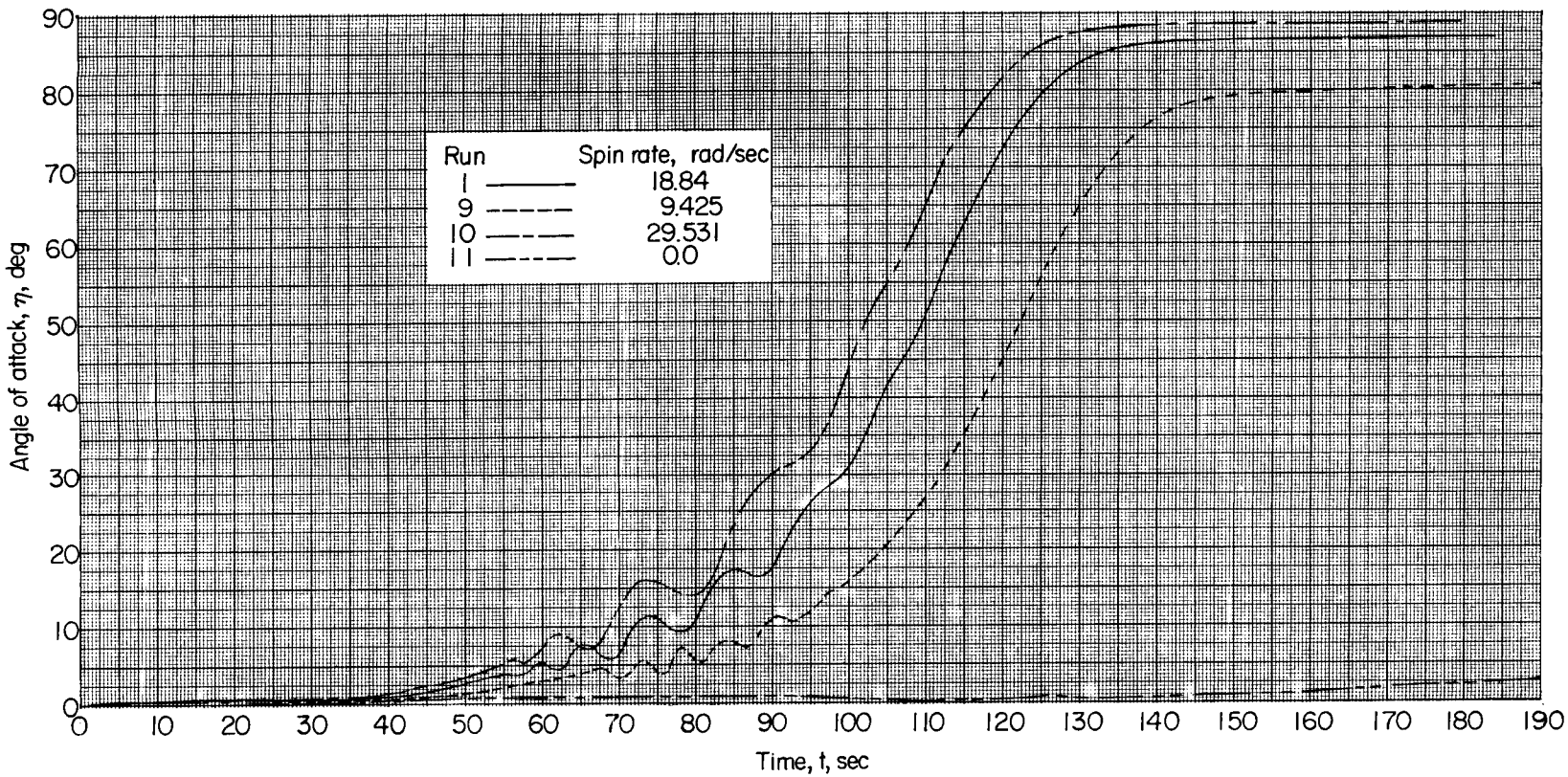

(a) Variation for the full reentry time.

Figure 12.- Effect of rate of spin on the angle-of-attack variation with time for the Project Fire reentry vehicle.

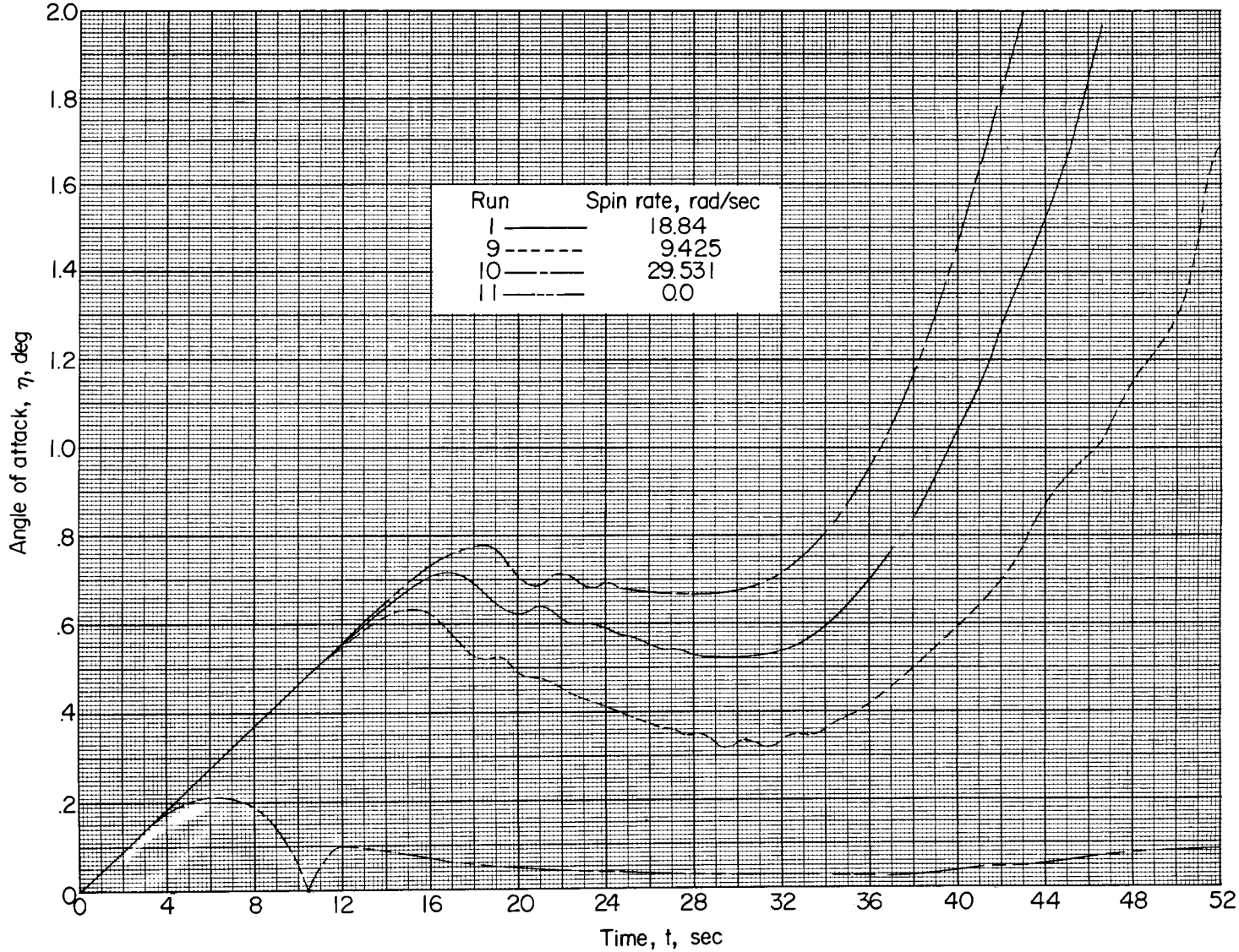

(b) Variation for the first 50 seconds of reentry.

Figure 12.- Concluded.

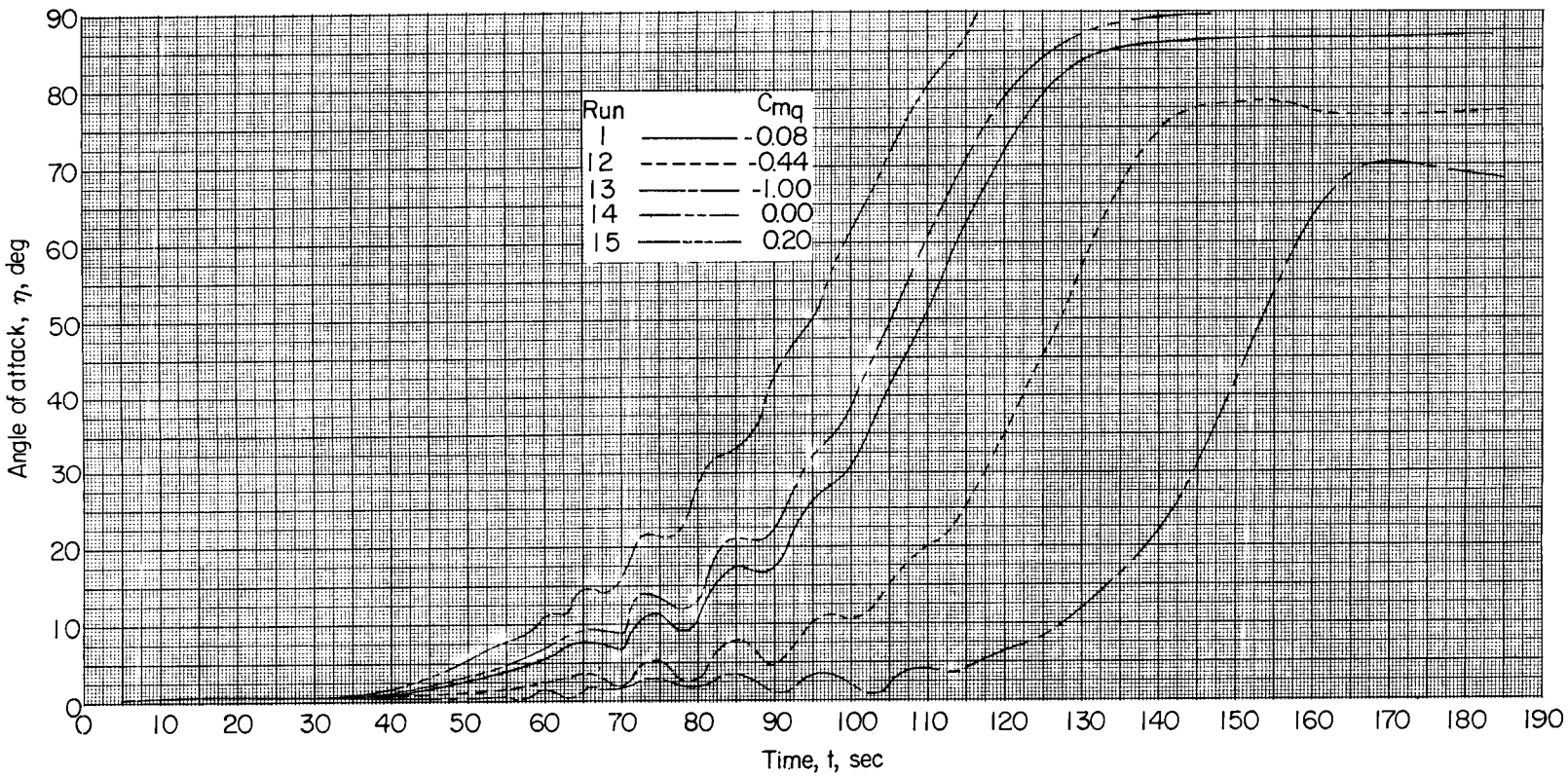

(a) Variation for the full reentry time.

Figure 13.- Effect of aerodynamic damping-moment coefficient on the angle-of-attack variation with time for the Project Fire reentry vehicle.

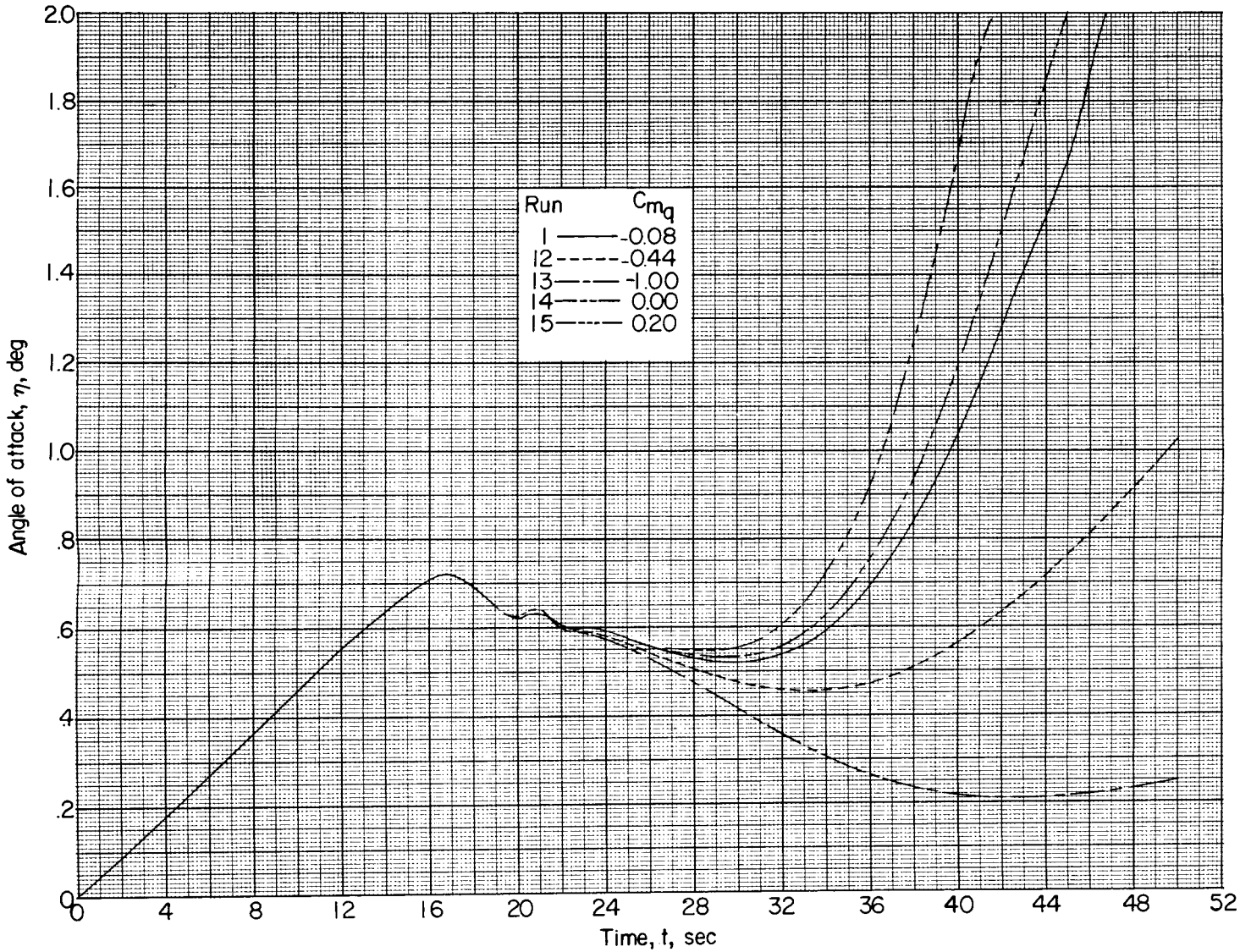

(b) Variation for the first 50 seconds of reentry.

Figure 13.- Concluded.

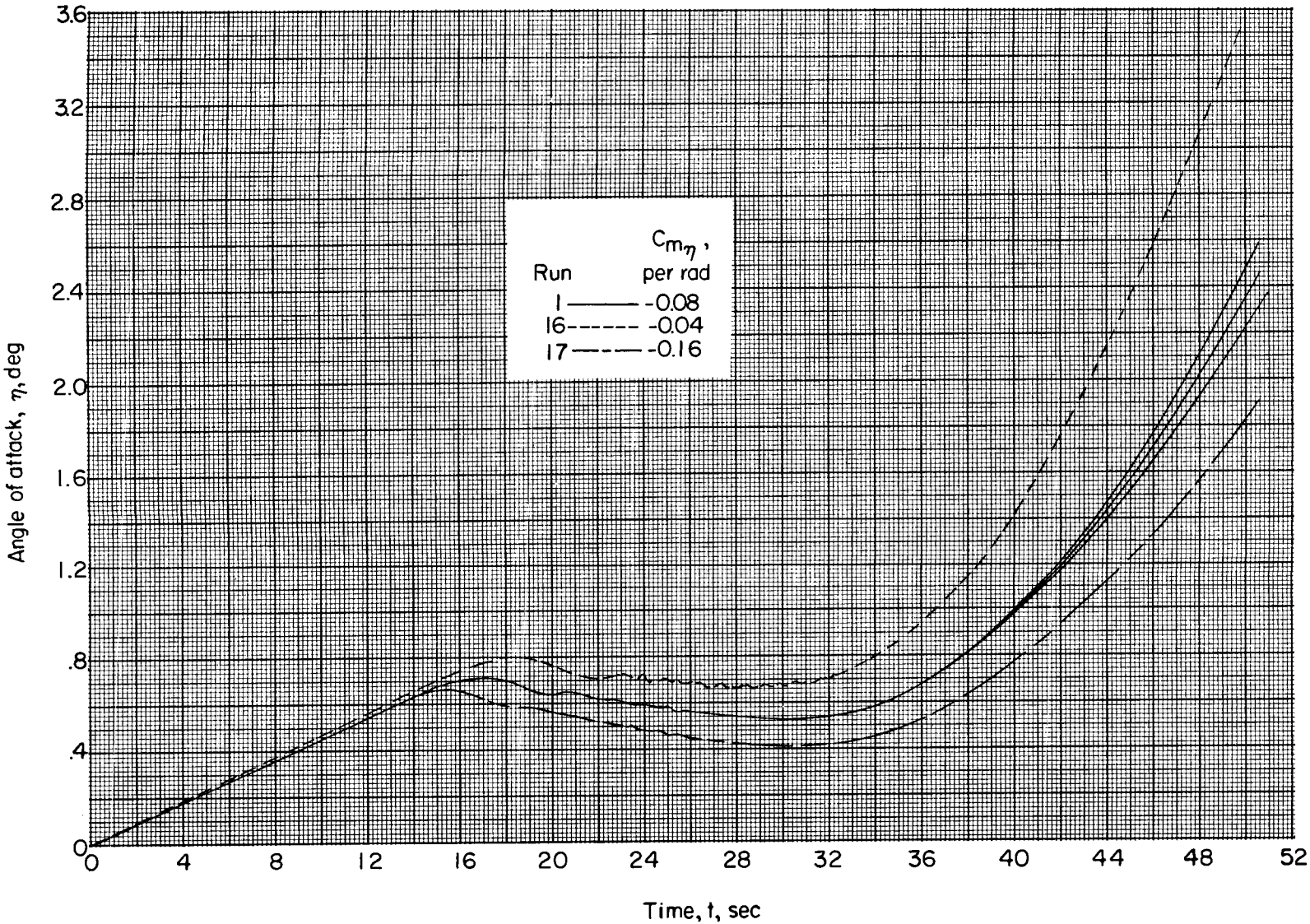

Figure 14.- Effect of static-stability coefficient on the angle-of-attack variation with time for the Project Fire reentry vehicle.

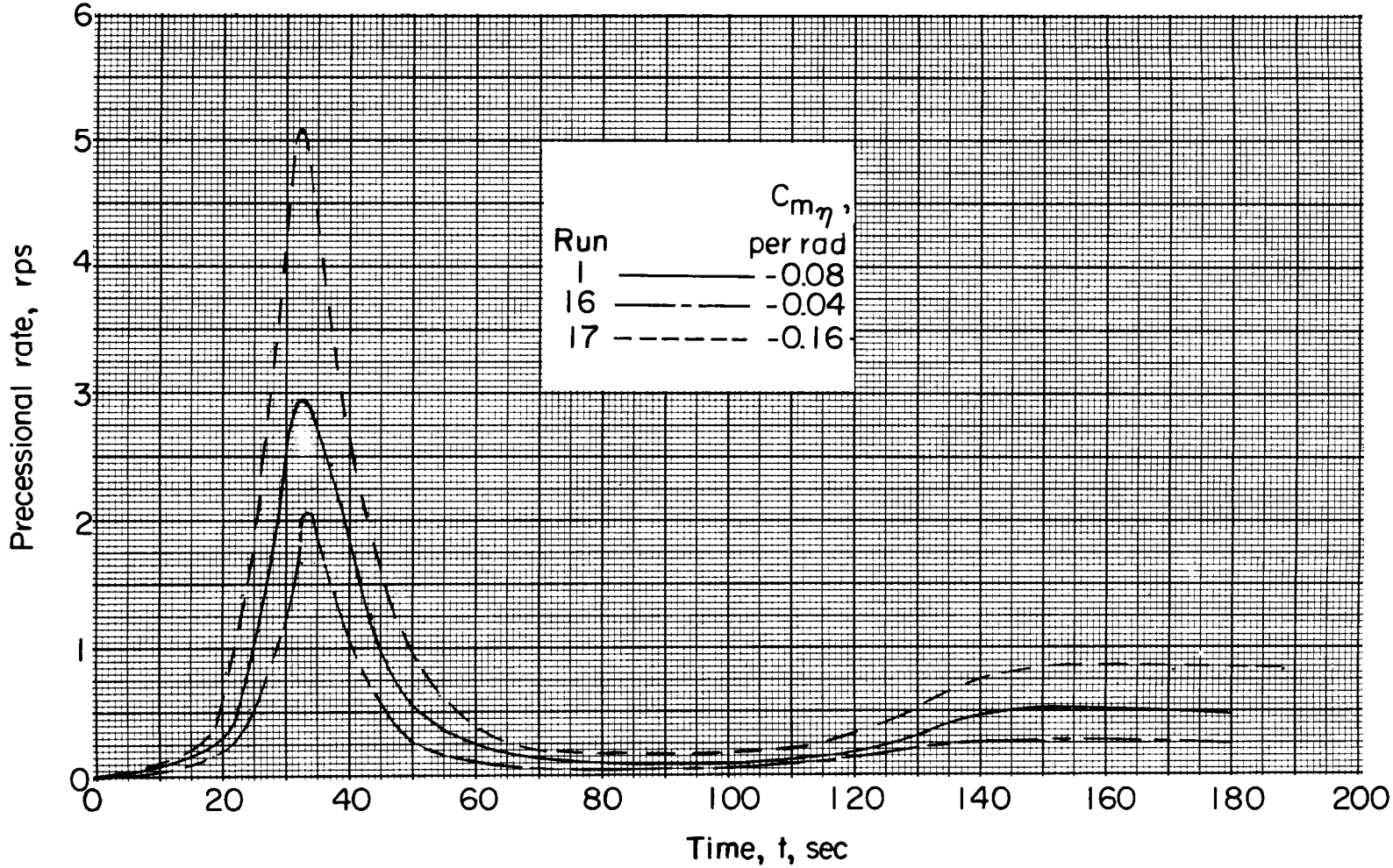

Figure 15.- Variation of precessional rate with time for three static-stability coefficients.

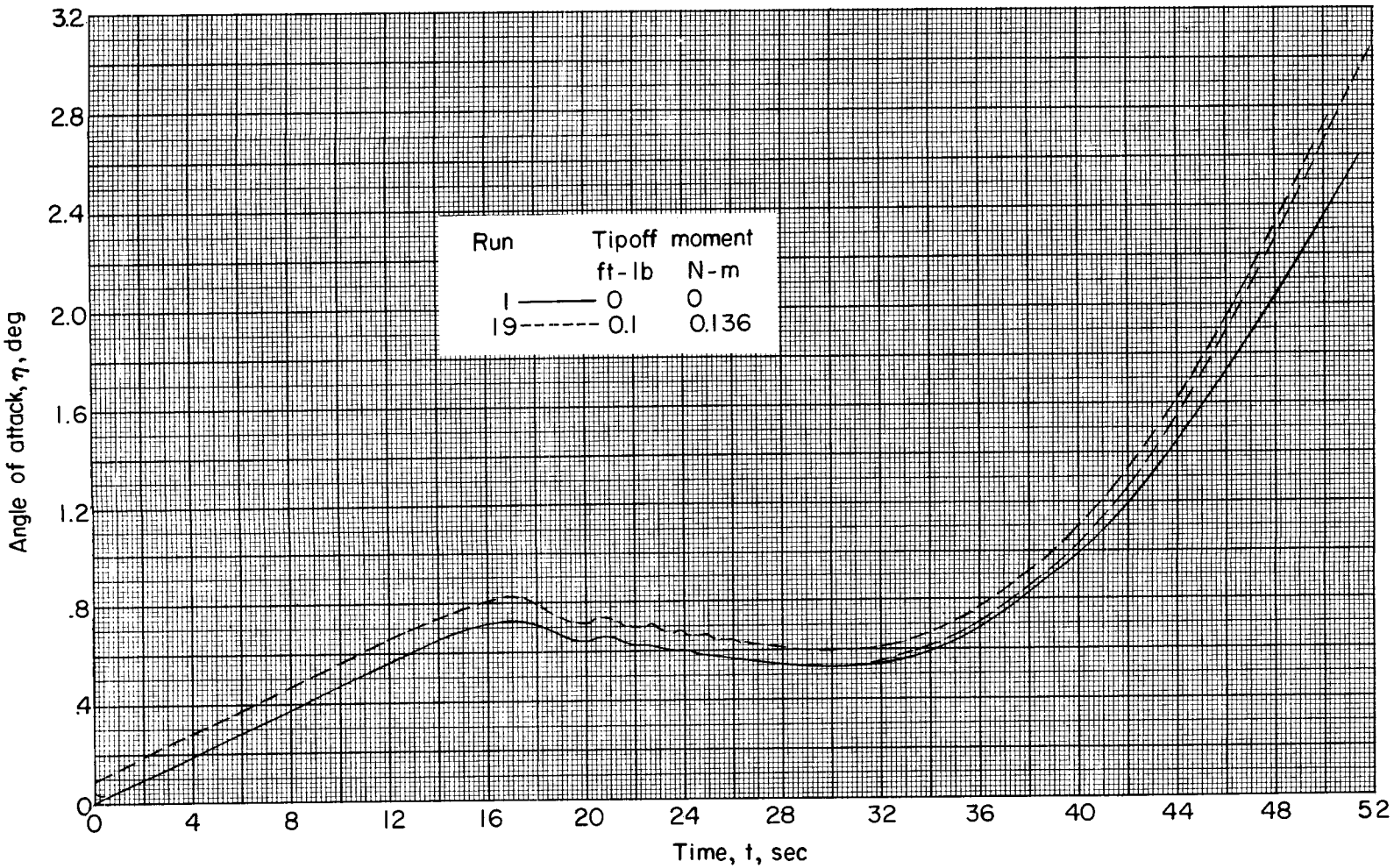

(a) Variation for 0 and 0.1 ft-lb applied for 1 second. The lower limit for run 19 coincides with run 1 for about the first 32 seconds.

Figure 16.- Effect of tipoff moment on the angle-of-attack variation with time for the Project Fire reentry vehicle. The double lines indicate the angle-of-attack envelope.

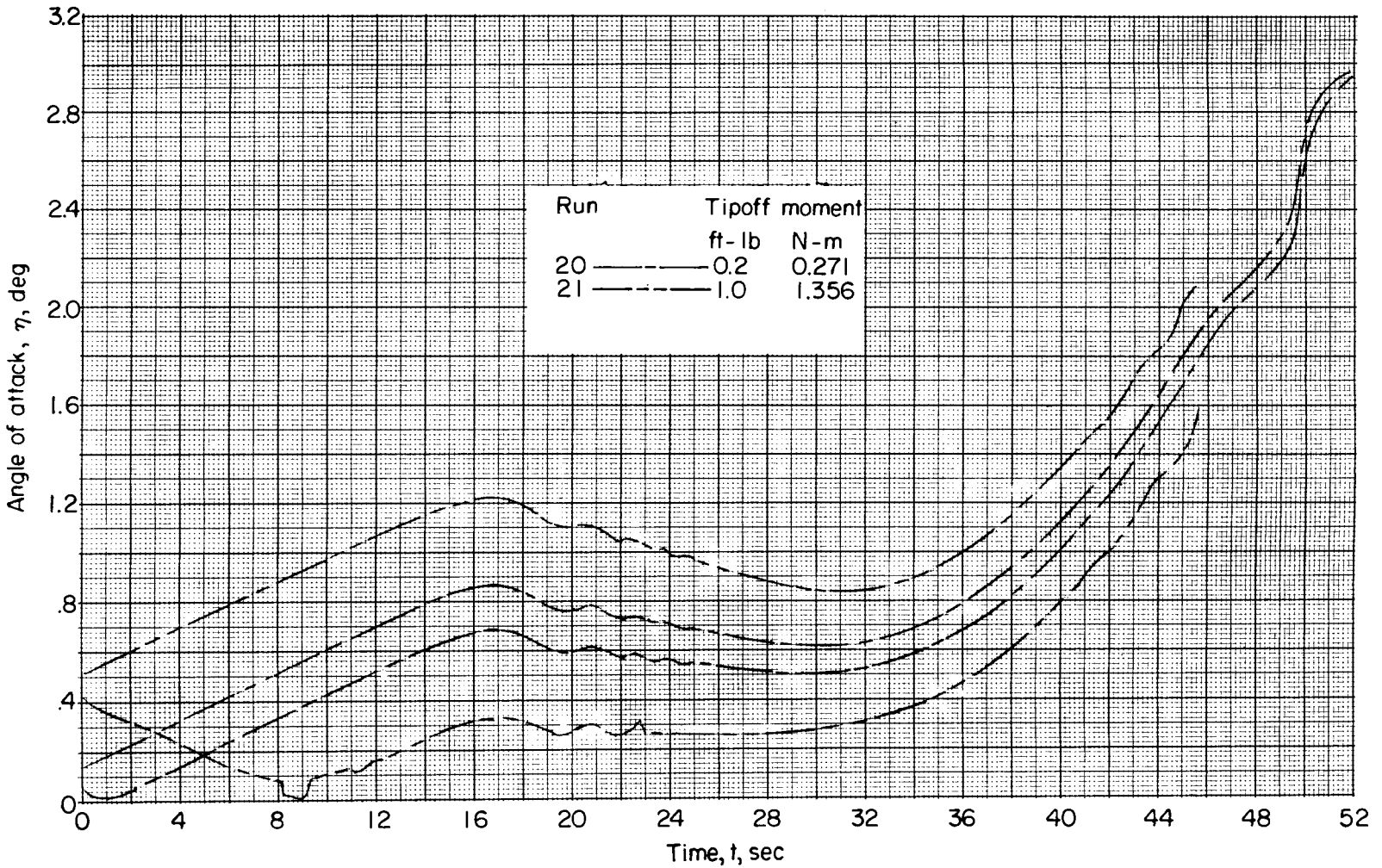

(b) Variation for 0.2 and 1.0 ft-lb applied for 1 second.

Figure 16.- Concluded.

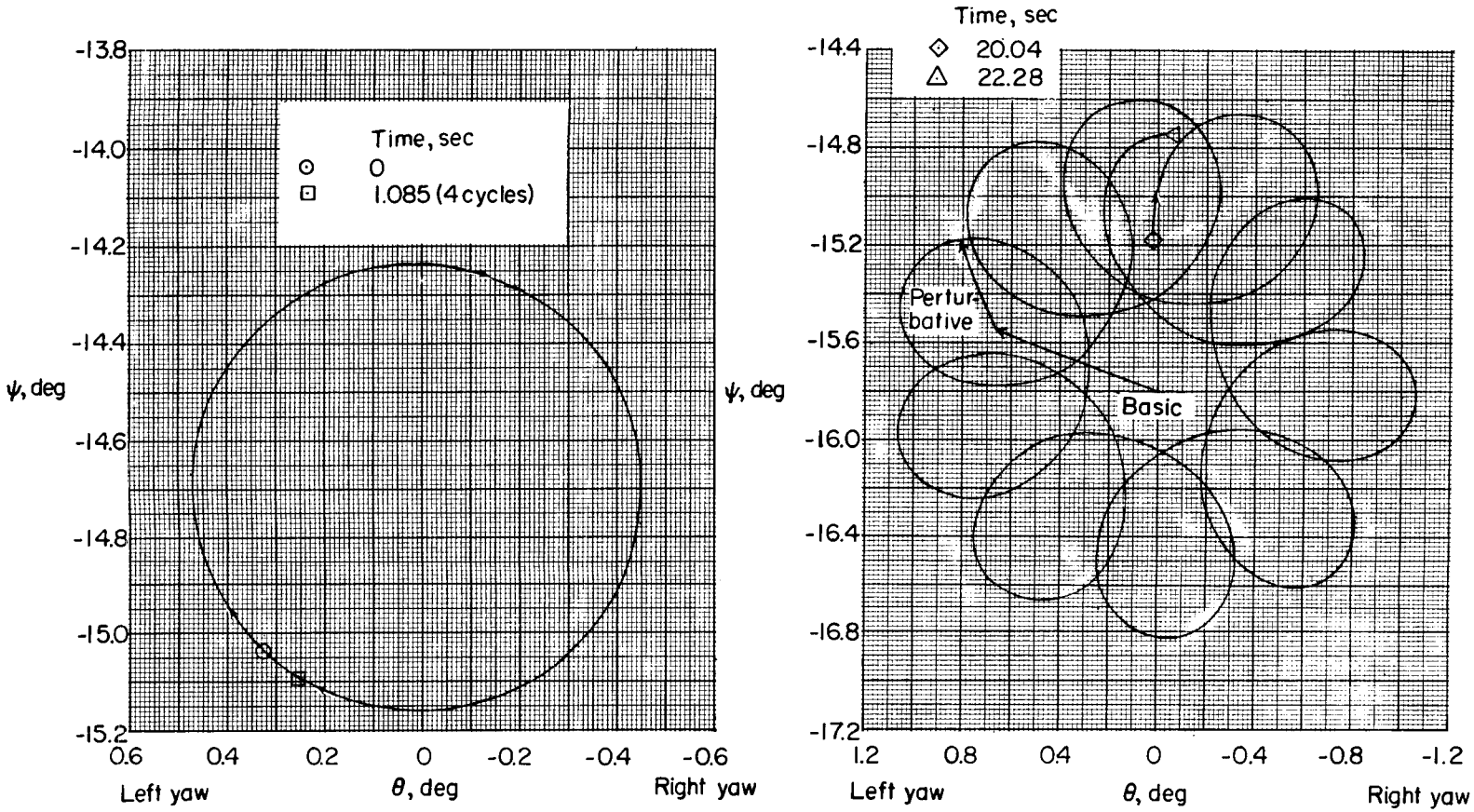

(a) Time from 0 to 1.085 seconds.

(b) Time from 20.04 to 22.28 seconds.

Figure 17.- Variation of yaw angle with pitch angle during four time periods throughout the run with tipoff moment of 1.0 ft-lb (1.356 N-m). (Run 21.) Vectors represent the magnitudes of the basic and perturbative motions.

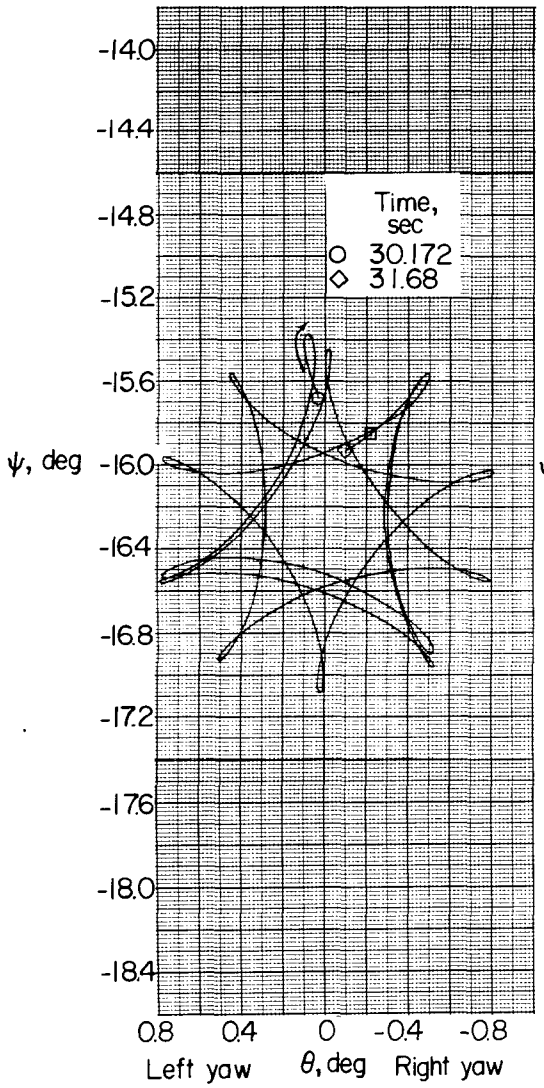

(c) Time from 30.172 to 31.68 seconds.

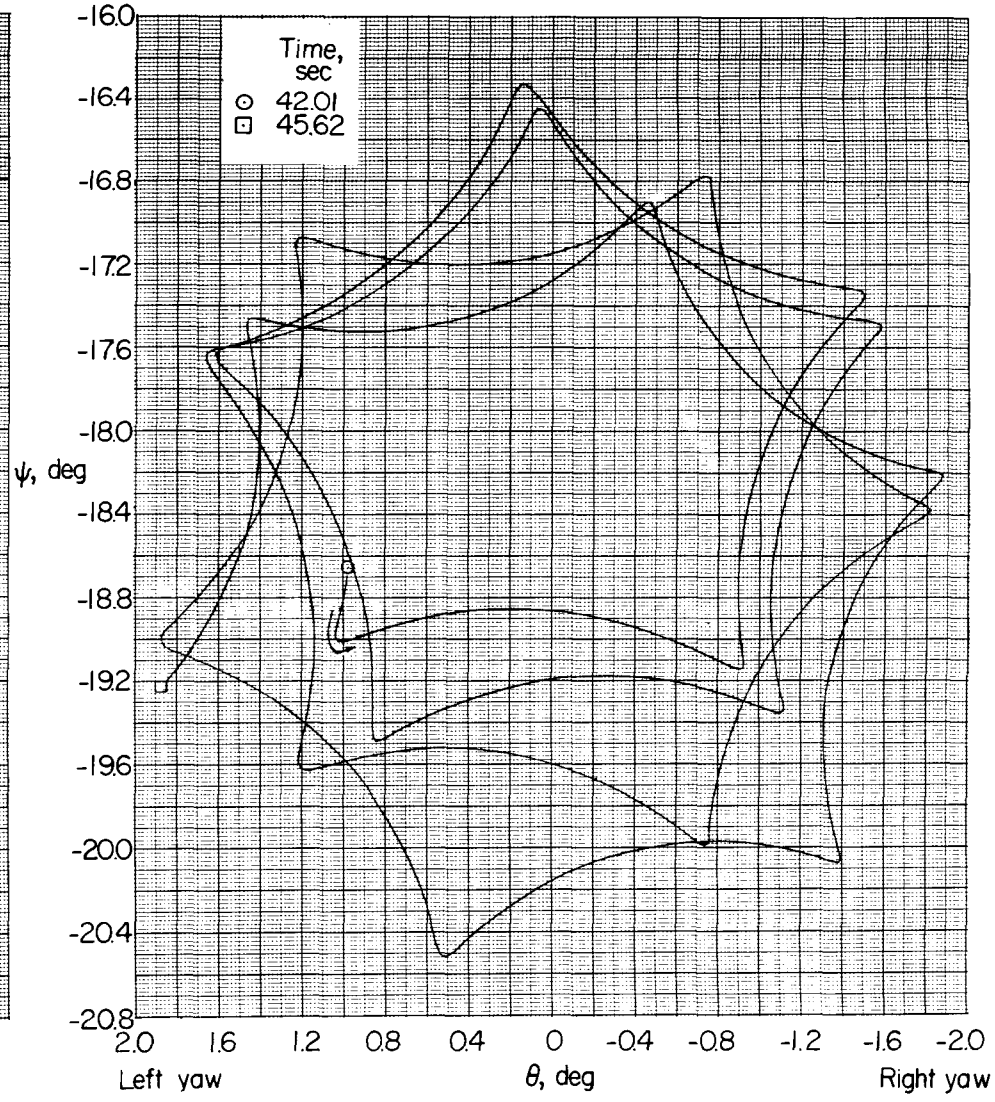

(d) Time from 42.01 to 45.62 seconds.

Figure 17.- Concluded.

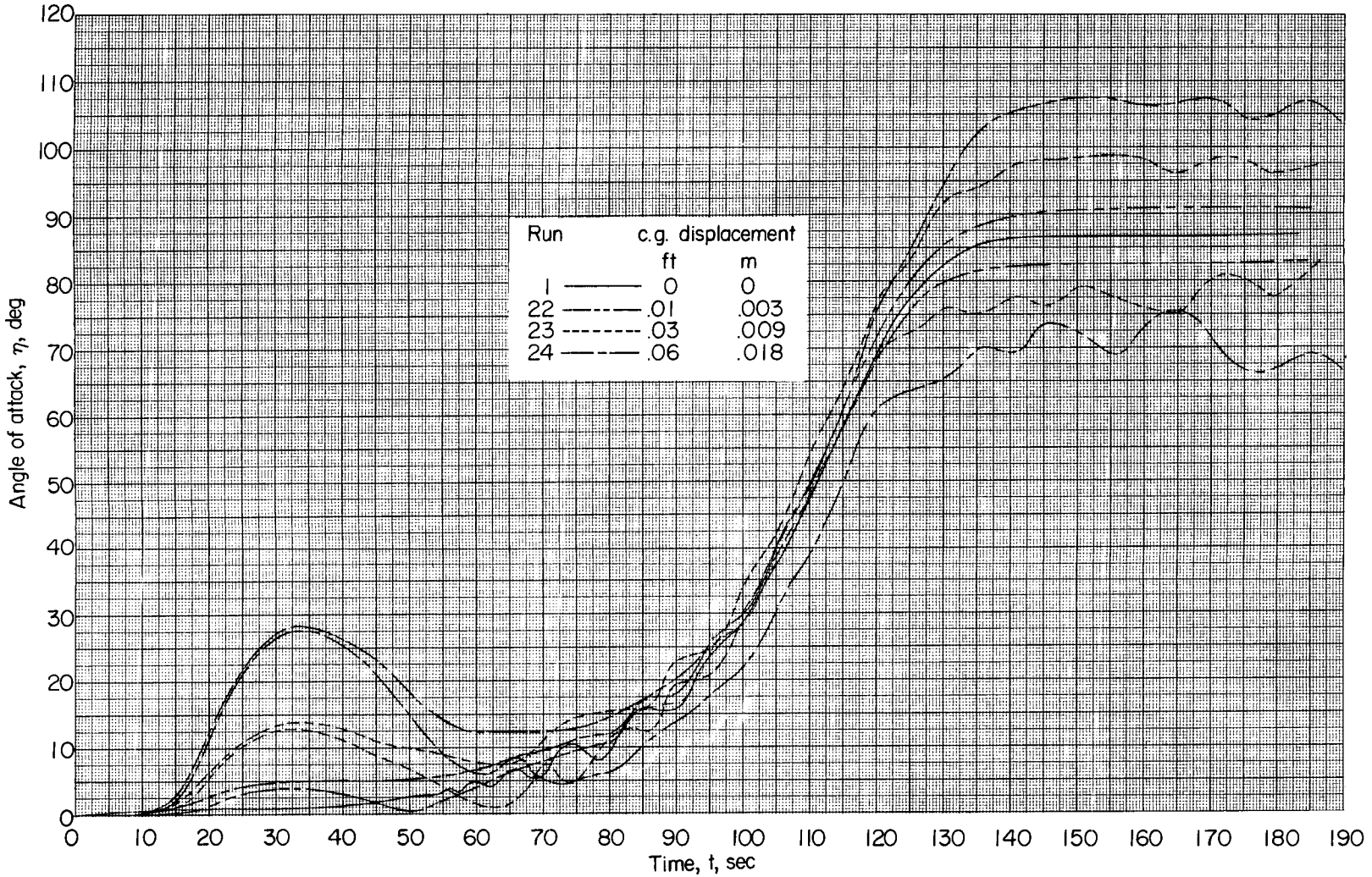

(a) Variation for the full reentry time.

Figure 18.- Effect of center-of-gravity displacement from the axis of symmetry on the angle-of-attack variation with time for the Project Fire reentry vehicle. Double lines indicate the angle-of-attack envelopes.

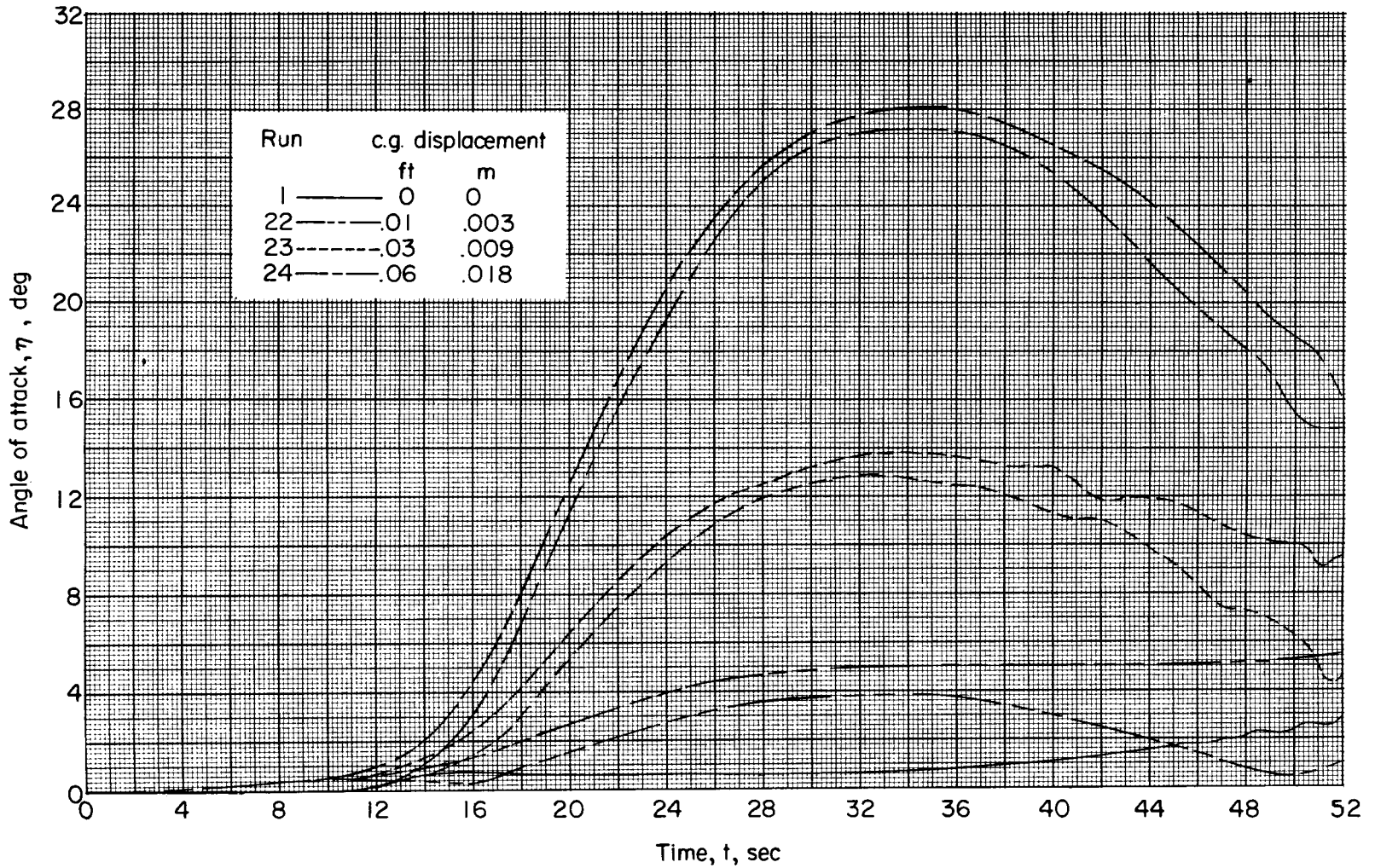

(b) Variation for the first 52 seconds of reentry.

Figure 18.- Concluded.

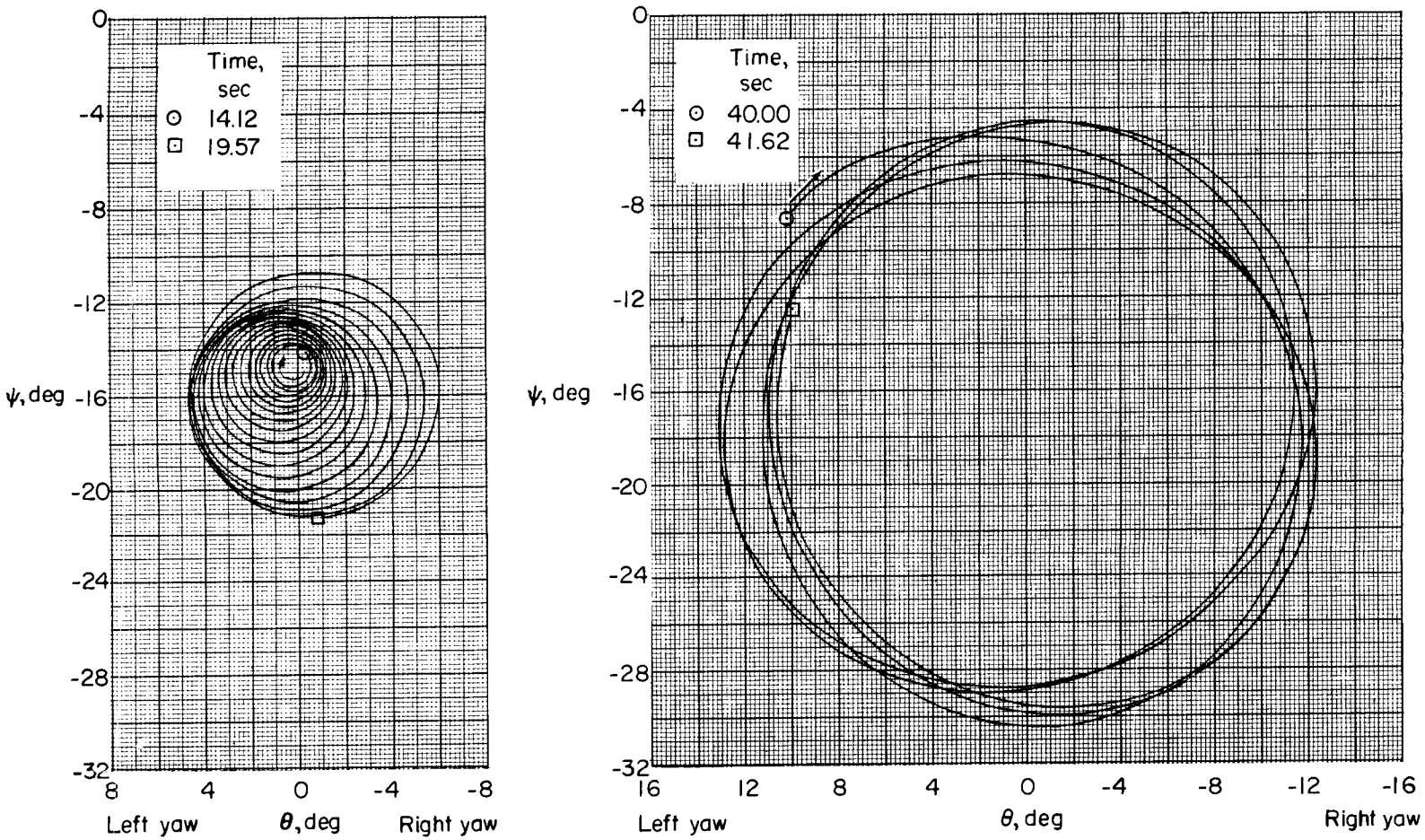

(a) Time from 14.12 to 19.57 seconds.

(b) Time from 40.00 to 41.62 seconds.

Figure 19.- Variation of yaw angle with pitch angle during three time periods throughout the run with the center of gravity off the axis of symmetry by 0.03 foot (0.009 meter). (Run 23.)

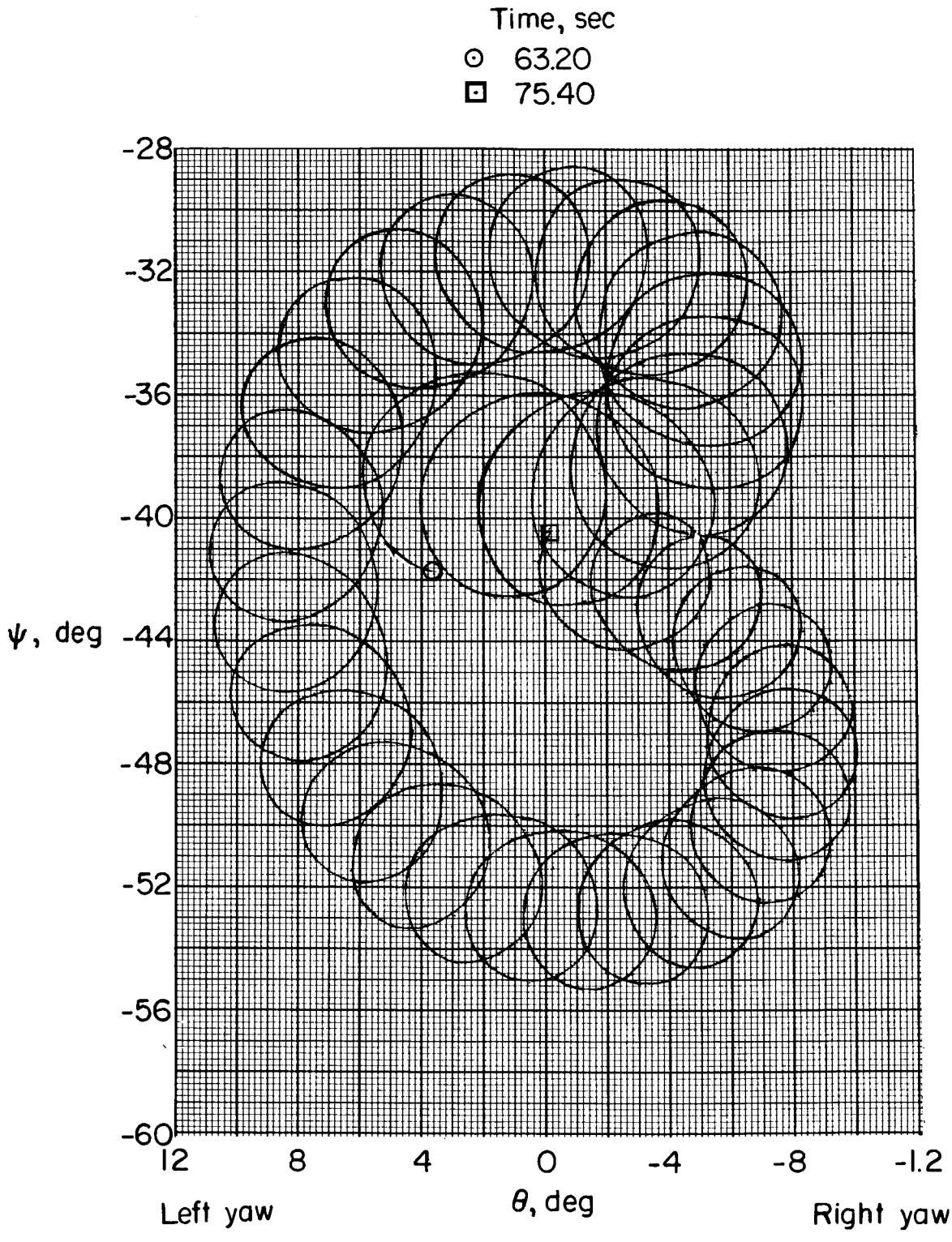

(c) Time from 63.20 to 75.40 seconds.

Figure 19.- Concluded.

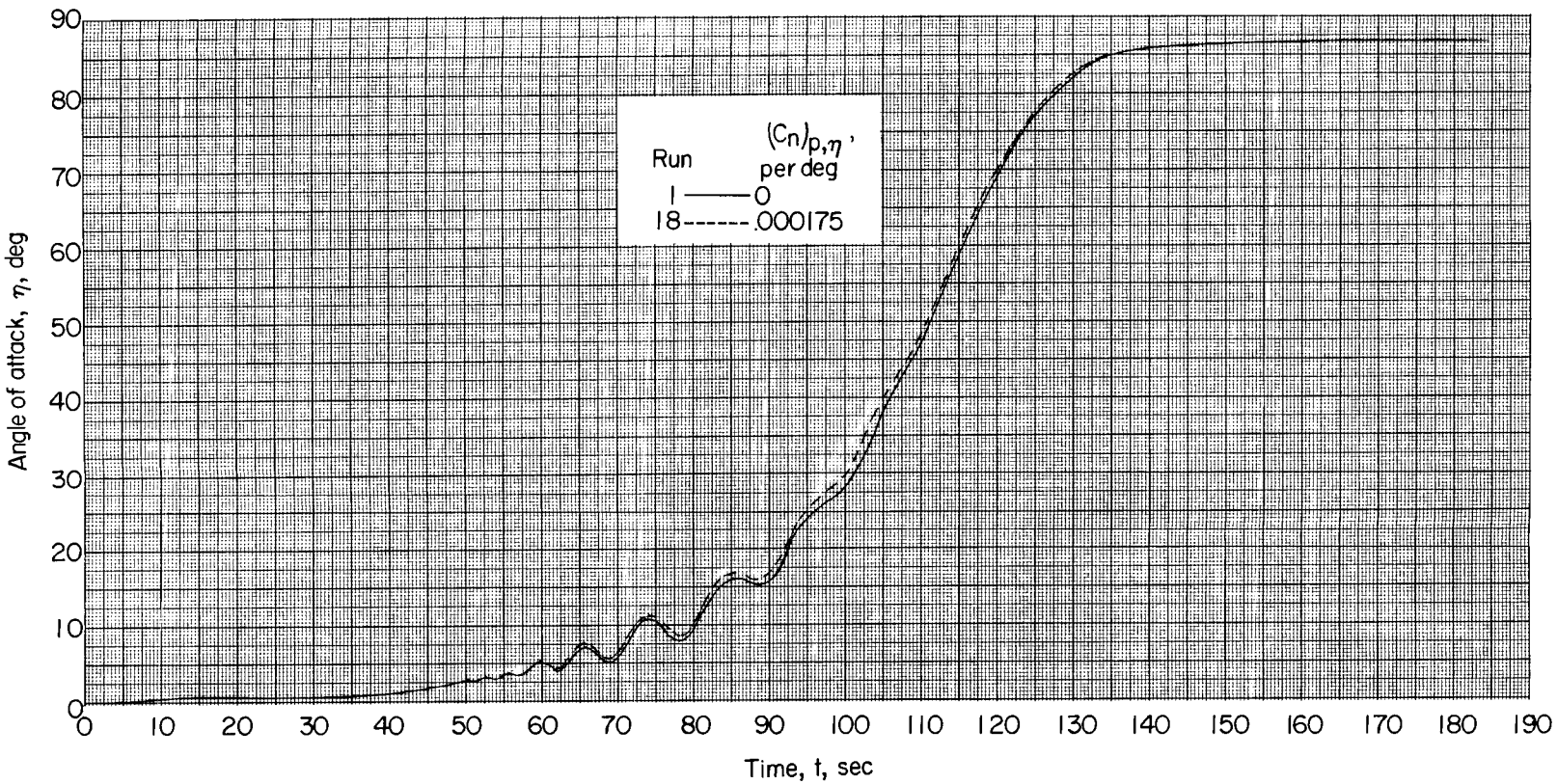

(a) Variation for the full reentry time.

Figure 20.- Effect of Magnus moment on the angle-of-attack variation with time for the Project Fire reentry vehicle.

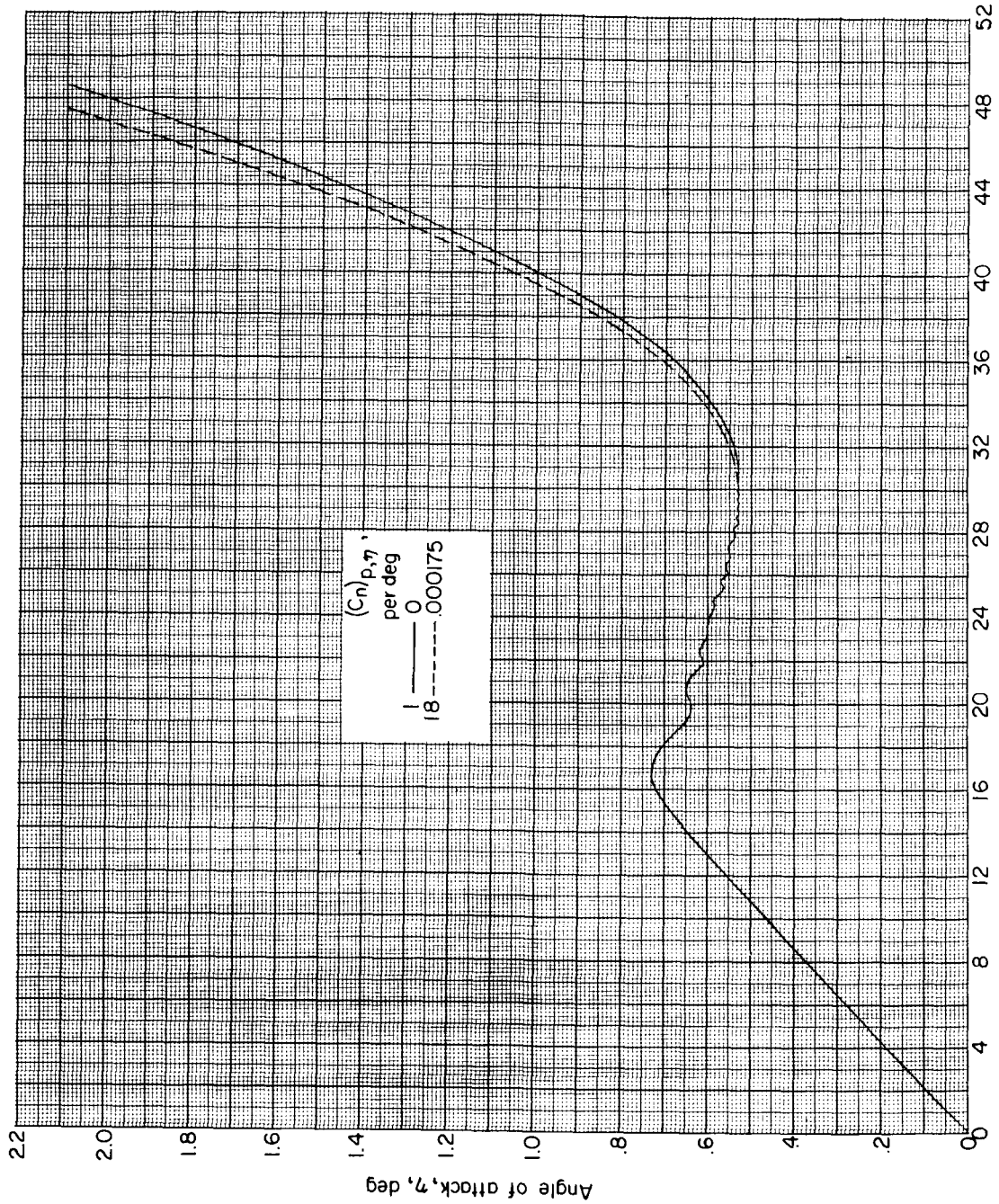

(b) Variation for the first 50 seconds of reentry.

Figure 20.- Concluded.

NASA-Langley, 1968 —— 31 L-5723

"The aeronautical and space activities of the United States shall be conducted so as to contribute . . . to the expansion of human knowledge of phenomena in the atmosphere and space. The Administration shall provide for the widest practicable and appropriate dissemination of information concerning its activities and the results thereof."

—NATIONAL AERONAUTICS AND SPACE ACT OF 1958

NASA SCIENTIFIC AND TECHNICAL PUBLICATIONS

TECHNICAL REPORTS: Scientific and technical information considered important, complete, and a lasting contribution to existing knowledge.

TECHNICAL NOTES: Information less broad in scope but nevertheless of importance as a contribution to existing knowledge.

TECHNICAL MEMORANDUMS: Information receiving limited distribution because of preliminary data, security classification, or other reasons.

CONTRACTOR REPORTS: Scientific and technical information generated under a NASA contract or grant and considered an important contribution to existing knowledge.

TECHNICAL TRANSLATIONS: Information published in a foreign language considered to merit NASA distribution in English.

SPECIAL PUBLICATIONS: Information derived from or of value to NASA activities. Publications include conference proceedings, monographs, data compilations, handbooks, sourcebooks, and special bibliographies.

TECHNOLOGY UTILIZATION PUBLICATIONS: Information on technology used by NASA that may be of particular interest in commercial and other non-aerospace applications. Publications include Tech Briefs, Technology Utilization Reports and Notes, and Technology Surveys.

Details on the availability of these publications may be obtained from:

SCIENTIFIC AND TECHNICAL INFORMATION DIVISION

NATIONAL AERONAUTICS AND SPACE ADMINISTRATION

Washington, D.C. 20546